

Degenerate quantum erasure decoding

Kao-Yueh Kuo^{1,*} and Yingkai Ouyang^{1,†}

¹*School of Mathematical and Physical Sciences, University of Sheffield, Sheffield, S3 7RH, United Kingdom*

Erasures are the primary type of errors in physical systems dominated by leakage errors. While quantum error correction (QEC) using stabilizer codes can combat these error, the question of achieving near-capacity performance with explicit codes and efficient decoders remains a challenge. Quantum decoding is a classical computational problem that decides what the recovery operation should be based on the measured syndromes. For QEC, using an accurate decoder with the shortest possible runtime will minimize the degradation of quantum information while awaiting the decoder's decision. We examine the quantum erasure decoding problem for general stabilizer codes and present decoders that not only run in linear-time but are also accurate. We achieve this by exploiting the symmetry of degenerate errors. Numerical evaluations show near maximum-likelihood decoding for various codes, achieving capacity performance with topological codes and near-capacity performance with non-topological codes. We furthermore explore the potential of our decoders to handle other error models, such as mixed erasure and depolarizing errors, and also local deletion errors via concatenation with permutation invariant codes.

I. INTRODUCTION

Erasure conversion is a recently developed technique which converts leakage errors into erasure errors. In physical systems dominated by leakage errors, such as ultracold Rydberg atoms [1–5], superconducting circuits [6–8], or photonic systems [9], erasure conversions ensure that the majority of the errors are erasure errors. In the context of quantum error correction (QEC), the promised structure of the errors affords potentially better decoder error thresholds and computational complexities than for errors with an unstructured form. In view of this, we would like to understand what the best QEC performance achievable in physical systems dominated by erasure errors is.

The rate of a QEC code is the ratio of the number of encoded qubits k to the number of physical qubits n . The capacity $C(p)$ of the quantum erasure channel which erases each qubit independently with probability p , is the maximal rate (k/n) for which there exists a decoder that almost surely corrects the typical erasures. This erasure capacity $C(p) = 1 - 2p$ [10] quantifies the ultimate rate at which quantum information can be reliably transmitted over identical uses of a noisy erasure channel. In practice, the rate at which a QEC code can reliably transmit over an erasure channel could be far less than the erasure capacity. A natural QEC question in the context of quantum information theory is then: how close can the reliable rate of transmission of practical QEC codes approach $C(p)$?

The above question is particularly pertinent for quantum stabilizer codes with code parameters $[[n, k]]$ and with checks given as low-weight Pauli operators. Such QEC codes, which admit low complexity QEC quantum circuits, are quantum low-density parity-check (QLDPC) codes, and include CSS- and non-CSS-type (e.g., XZZX) topological codes [11–14], [15–17], bicycle codes [18], hypergraph-product (HP) codes [19], generalized HP (GHP) codes [20],

lifted-product (LP) codes [21], etc. QLDPC codes offer the attractive features of (1) enabling error-corrected quantum computation with a constant encoding rate [22, 23] and (2) enhancing quantum network communication rates [24].

In the QEC of stabilizer codes, one measures check operators on the quantum state and applies a quantum channel based on the measurement outcome. The decoder in QEC is an algorithm that decides what the applied quantum channel should be, based on the measurement outcome, called the syndrome. In practical QEC, the quality of the decoding decision must be balanced with how fast the decision is made, to prevent too many errors from accumulating while awaiting the decoder's decision.

The decoder in QEC that makes the optimal decision is the maximal-likelihood decoder (MLD). The MLD for stabilizer codes reduces the problem of decoding erasure errors on stabilizer codes to that of solving a system of linear equations, and can use Gaussian elimination at its core. Hence, the MLD has a runtime complexity of $O(n^3)$. In the context of classical erasure correction, the binary bit-flipping belief-propagation (Flip-BP₂) decoder instead of the MLD is widely used on classical LDPC codes (with great success in today's 5G networks [25, 26]), because Flip-BP₂ accurately approximates the optimal decoding decision in linear time $O(n)$ [27–33]. On QLDPC codes however, a naive application of Flip-BP₂ is problematic; when decoding QLDPC codes using Flip-BP₂, one inevitably encounters harmful stopping sets [34], and stopping sets prevent the convergence of BP decoding [29–33, 35, 36]. Classical LDPC codes avoid this stopping set problem in the code design [30–33].

Since Flip-BP₂ has the attractive feature of a linear runtime complexity, variants of Flip-BP₂ have been designed specifically for decoding QLDPC codes. First, similar to a Flip-BP₂ technique [28], the peeling decoder was proposed to decode toric and surface codes, to achieve MLD, while keeping the linear-time efficiency [37]. The peeling decoder was also extended to decode color codes [38–40]. Toric, surface, and color codes are topological codes with asymptotically zero code rate. Second, to decode HP codes with good performance, the pruned peeling which improves on the peeling decoder and a post-processing named

* k.kuo@sheffield.ac.uk

† y.ouyang@sheffield.ac.uk

Vertical-Horizontal (VH) decoder was proposed [34]. The “pruned peeling + VH” complexity is $O(n^2)$, or is $O(n^{1.5})$ for a probabilistic version of this decoder. Third, modifications of minimum-weight perfect matching (MWPM) can have good erasure decoding performance for certain QEC codes [41, 42], but cannot decode in linear time [43]. Finally, note that the previous literature primarily focused on low-rate topological or HP codes [34, 37–40].

We aim to introduce BP-based decoders that not only have good performance for general stabilizer codes, such as high rate QLDPC codes, but are furthermore also efficient in runtime complexity. The optimal decision of our decoder for a given syndrome is not a fixed error; convergence onto any one of the degenerate errors that correspond to the syndrome would suffice.

In this paper, we introduce a gradient-descent Flip-BP₂ (GD Flip-BP₂), using a simple GD scheme to overcome stopping sets. The symmetry of degenerate errors, discussed in [44] and further examined in this paper, supports the effectiveness of this GD method, enabling BP to carry out effective correction. On the other hand, we use a quaternary soft-valued BP with memory effects (MBP₄) and its adaptive version (AMBP₄) from [45]. For this, we modify the decoder input and handle erasure decoding like a soft GD optimization. (A)MBP₄ are derived from a GD optimization using the soft information from all checks, significantly improving the convergence over the vanilla Flip-BP₂ decoder. Our BP-based decoders show numerically that the optimal rates of various families of QLDPC codes approach $1 - 2.5p$, demonstrating the potential of our BP decoders.

BP is an iterative decoder, where each iteration takes linear time. On classical codes, the average number of BP iterations expected for convergence is $O(\log \log n)$ [46, 47], which is essentially constant time. For low logical error rate regions of interest, we observe a similar rate of convergence for the QLDPC codes we study. BP needs a message update schedule. Typically, a parallel schedule is used. We also consider a group schedule [45, arXiv Sec. 5]. The group schedule has strong parallelism, with some non-parallelism, which prevents decoding oscillation with improved convergence [45, 48]. Furthermore, randomising group schedule minimises the chance of syndromes causing the decoder to be trapped by the same stopping set. We show that this random group schedule significantly improves the performance for many QLDPC codes.

For decoders, we propose a straightforward criterion to assess if a decoder approximates MLD closely. Using this criterion, we observe that (A)MBP₄ performs near MLD across various quantum codes. Additionally, GD Flip-BP₂, though simple, achieves performance comparable to (A)MBP₄ on many bicycle and LP codes. This is practically important, as GD Flip-BP₂ has very low complexity, and both bicycle and LP codes support flexible code lengths and rates.

For long codes, we estimate a code family’s error threshold p_{th} by evaluating if long-code performance aligns with a sphere-packing bound criterion, which indicates exponential decay in logical error rate at $p < p_{\text{th}}$ as n grows.

Finally, we explore the potential of our decoders to man-

age erasure, deletion (with the assistance of permutation invariant (PI) codes [49, 50]), and depolarizing errors.

We begin our paper by introducing stabilizer codes and the quantum erasure decoding problem in Sec. II. We give further insight into the decoding problem using group theory and probability theory in Sec. III. We present our decoding algorithms in Sec. IV, followed by simulation results in Sec. V. Finally, we conclude in Sec. VI.

II. STABILIZER CODES AND ERASURE DECODING

A quantum code encoding k information qubits to n physical qubits is an $[[n, k]]$ code. An $[[n, k]]$ code that is stabilized (fixed) by $n - k$ independent and commuting n -fold Pauli operators is an $[[n, k]]$ stabilizer code [51, 52]. The set of all operators generated by the $n - k$ independent generators form a subgroup \mathcal{S} of the n -fold Pauli group $\mathcal{P}_n = \{cE_1 \otimes E_2 \otimes \dots \otimes E_n : c \in \{\pm 1, \pm i\}, E_j \in \{I, X, Y, Z\} \forall j\}$, where $I = \begin{bmatrix} 1 & 0 \\ 0 & 1 \end{bmatrix}$, $X = \begin{bmatrix} 0 & 1 \\ 1 & 0 \end{bmatrix}$, $Y = \begin{bmatrix} 0 & -i \\ i & 0 \end{bmatrix}$, and $Z = \begin{bmatrix} 1 & 0 \\ 0 & -1 \end{bmatrix}$. The subgroup \mathcal{S} is called the *stabilizer group*. Elements in \mathcal{S} are called *stabilizers*. We represent the independent generators of \mathcal{S} as $H^{(1)}, H^{(2)}, \dots, H^{(n-k)}$.

Elements in \mathcal{P}_n have eigenvalues ± 1 . Two elements E, F in \mathcal{P}_n either commute $EF = FE$ or anticommute $EF = -FE$. The stabilizer code stabilized by \mathcal{S} , denoted by $\mathcal{C}(\mathcal{S})$, is the joint $+1$ subspace of $\{H^{(i)}\}_{i=1}^{n-k}$ in $\{|0\rangle, |1\rangle\}^{\otimes n}$.

The error discretization theorem allows us to focus on the set of Pauli errors \mathcal{P}_n [53]. When an unknown Pauli error E acts on a code state $|v\rangle \in \mathcal{C}(\mathcal{S})$, for decoding, we measure the observables $\{H^{(i)}\}_{i=1}^{n-k}$. The measurement outcome of each $H^{(i)}$ is either $+1$ or -1 . We collect the measurement outcomes in a vector $s = (s_1, \dots, s_n) \in \{+1, -1\}^{n-k}$, where $s_i = 1$ if $EH^{(i)} = H^{(i)}E$, and $s_i = -1$ if $EH^{(i)} = -H^{(i)}E$. The decoding is a procedure using s to infer E , which is a classical computational problem.

We ignore the global phase and the tensor-product, and represent the observables $\{H^{(i)}\}_{i=1}^{n-k}$ as a *Pauli check matrix*

$$H = \begin{bmatrix} H^{(1)} \\ \vdots \\ H^{(n-k)} \end{bmatrix} \in \{I, X, Y, Z\}^{(n-k) \times n}, \quad (1)$$

which is a quaternary check matrix [51]. A row in a check matrix is called a *check*. It is possible to put additional stabilizers to have more than $n - k$ checks.

In the following, $\mathbf{0}$ and $\mathbf{1}$ denote the zero and identity matrices of appropriate dimensions, respectively. Similarly, $\mathbf{0}_n$ and $\mathbf{1}_n$ represent the $n \times n$ zero and identity matrices, respectively. We denote the cardinality of a set a by $|a|$.

A. Stabilizer decoding problem

Representing H in (1) as a binary matrix allows us to derive a linear code, by using a group homomorphism $\varphi : \mathcal{P}_n \rightarrow \{0, 1\}^{2n}$ with kernel $\{\pm \mathbf{1}, \pm i \mathbf{1}\} \subset \mathcal{P}_n$ [52, 54, 55]. The group homomorphism φ ignores the global phase

and maps $E = E_1 \otimes \cdots \otimes E_n \in \mathcal{P}_n$ component-wise to $\mathbf{E} = (\mathbf{E}^X | \mathbf{E}^Z) = (\mathbf{E}_1^X, \dots, \mathbf{E}_n^X | \mathbf{E}_1^Z, \dots, \mathbf{E}_n^Z) \in \{0, 1\}^{2n}$. Here, $(\mathbf{E}_j^X | \mathbf{E}_j^Z) = (0|0), (1|0), (0|1), (1|1)$ if $E_j = I, X, Z, Y$, respectively, for $j = 1, 2, \dots, n$.

We can check the operator commutativity in the vector space. For two binary matrices \mathbf{A} and \mathbf{B} of $2n$ columns, define a bilinear form (called *symplectic inner product*)

$$\langle \mathbf{A}, \mathbf{B} \rangle = \mathbf{A} \mathbf{\Lambda} \mathbf{B}^T,$$

where $\mathbf{\Lambda} = \begin{bmatrix} 0_n & \mathbf{1}_n \\ \mathbf{1}_n & 0_n \end{bmatrix}$ and $(\cdot)^T$ is the matrix transpose. Two operators $E, F \in \mathcal{P}_n$ commute if the corresponding vectors $\mathbf{E}, \mathbf{F} \in \{0, 1\}^{2n}$ satisfy $\langle \mathbf{E}, \mathbf{F} \rangle = 0$, and anti-commute if $\langle \mathbf{E}, \mathbf{F} \rangle = 1$.

The image $\varphi(\mathcal{S})$ of the stabilizer group \mathcal{S} is a classical code $C \subset \{0, 1\}^{2n}$ that is self-orthogonal with respect to the symplectic inner product, i.e., if $\mathbf{u}, \mathbf{v} \in C$, then $\langle \mathbf{u}, \mathbf{v} \rangle = 0$. We construct a matrix to generate the code C . Let $\mathbf{H}_i = \varphi(H^{(i)}) \in \{0, 1\}^{2n}$ for $i = 1, 2, \dots, n-k$ and construct an $(n-k) \times 2n$ binary matrix

$$\mathbf{H} = \begin{bmatrix} \varphi(H^{(1)}) \\ \vdots \\ \varphi(H^{(n-k)}) \end{bmatrix} = \begin{bmatrix} \mathbf{H}_1 \\ \vdots \\ \mathbf{H}_{n-k} \end{bmatrix} = \begin{bmatrix} H_{1,1} & \cdots & H_{1,2n} \\ \vdots & \ddots & \vdots \\ H_{n-k,1} & \cdots & H_{n-k,2n} \end{bmatrix}. \quad (2)$$

An alternative representation of \mathbf{H} is

$$\mathbf{H} = [\mathbf{H}^X | \mathbf{H}^Z] = \begin{bmatrix} H_{1,1}^X & \cdots & H_{1,n}^X & | & H_{1,1}^Z & \cdots & H_{1,n}^Z \\ \vdots & \ddots & \vdots & | & \vdots & \ddots & \vdots \\ H_{n-k,1}^X & \cdots & H_{n-k,n}^X & | & H_{n-k,1}^Z & \cdots & H_{n-k,n}^Z \end{bmatrix}. \quad (3)$$

We have the code C the row-space of \mathbf{H} , i.e.,

$$\varphi(\mathcal{S}) = C = \text{Row}(\mathbf{H}).$$

We call \mathbf{H} a *binary check matrix* of the stabilizer code, which has full row-rank and is self-orthogonal, i.e., $\langle \mathbf{H}, \mathbf{H} \rangle = \mathbf{0}$.

We map the measurement outcomes $s \in \{+1, -1\}^{n-k}$ as a binary vector $\mathbf{s} \in \{0, 1\}^{n-k}$ by $s_i = 0$ if $s_i = +1$ and $s_i = 1$ if $s_i = -1$. We call \mathbf{s} the *syndrome* of the error $\mathbf{E} = \varphi(E)$, where E is the (unknown) Pauli error. Specifically, we have $\mathbf{s} = \langle \mathbf{E}, \mathbf{H} \rangle$.

We consider two types of decoding, optimized according to different maximum-likelihood criteria [56–58].

Definition 1. (*Classical-sense maximum-likelihood decoding (CMLD)*) Given \mathbf{H} (of a stabilizer code), \mathbf{s} (syndrome), and necessary information of the channel, where $\mathbf{s} = \langle \mathbf{E}, \mathbf{H} \rangle$ for some \mathbf{E} drawn from the channel, a CMLD finds an $\hat{\mathbf{E}} \in \{0, 1\}^{2n}$ maximizing this probability $\Pr(\hat{\mathbf{E}} = \mathbf{E})$.

The previous decoding criterion is not necessarily a true MLD criterion in the quantum case, as it relies on the classical criterion ($\hat{\mathbf{E}} = \mathbf{E}$) for error correction.

In the quantum case, two Pauli operators E, F up to a stabilizer effect the same logical operation on the code space. Their binary representations \mathbf{E}, \mathbf{F} satisfy $\mathbf{E} + \mathbf{F} \in C$, or equivalently, $\mathbf{F} \in \mathbf{E} + C$. In this case, we call \mathbf{F} a *degenerate error*

of \mathbf{E} . Since \mathbf{E} and \mathbf{F} correspond to the same logical operation, we define the *logical coset* of \mathbf{E} as

$$\mathbf{E} + C = \{\mathbf{F} \in \{0, 1\}^{2n} : \mathbf{F} + \mathbf{E} \in C\}. \quad (4)$$

This leads us to consider:

Definition 2. (*Quantum maximum-likelihood decoding (QMLD)*) Given \mathbf{H} (of a stabilizer code), \mathbf{s} (syndrome), and necessary information of the channel, where $\mathbf{s} = \langle \mathbf{E}, \mathbf{H} \rangle$ for some \mathbf{E} drawn from the channel model, a QMLD finds an $\hat{\mathbf{E}} \in \{0, 1\}^{2n}$ maximizing this probability $\Pr(\hat{\mathbf{E}} \in \mathbf{E} + C)$.

When we mention MLD, we refer to the criterion in Def. 2.

B. Quantum erasure channel

In some systems, a qubit (specifically, its information) is lost if it erroneously ends in an “erasure state” $|2\rangle$ orthogonal to the computation basis states $|0\rangle$ and $|1\rangle$ [10, 59]. In certain physical implementations, erasures occur when some qubits are lost, and the receiver, aided by a detector, can identify the location of each lost qubit [60]. A qubit, ρ_1 , once lost, is inserted (replaced) with an ancilla qubit, treated as a completely mixed state $\frac{1}{2}$ [53]:

$$\frac{1}{2} = \sum_{W \in \{I, X, Y, Z\}} \frac{1}{4} W \rho_1 W^\dagger. \quad (5)$$

This process is modelled as a quantum erasure channel [10, 59], where each qubit is independently erased with probability $p \in (0, 0.5)$. A non-erased qubit remains untouched. An erased qubit becomes completely mixed. The channel operation on a single qubit is given by

$$\rho_1 \mapsto (1-p)\rho_1 + p\frac{1}{2} \quad (6)$$

prior to determining whether the qubit is erased. However, the decoder is informed of which qubits are erased.

Definition 3. For a code of length n , let $\mathfrak{r} \subseteq \{1, 2, \dots, n\}$ represent the set of erased coordinates. If $j \in \mathfrak{r}$, then qubit j is erased. The complement, $\bar{\mathfrak{r}} = \{1, 2, \dots, n\} \setminus \mathfrak{r}$, contains the non-erased coordinates.

As a result, after stabilizer measurements are performed, each inserted ancilla qubit collapses randomly, encountering Pauli I, X, Y , or Z with equal probability $1/4$. For an $[[n, k]]$ code, a Pauli error $E = E_1 \otimes \cdots \otimes E_n \in \mathcal{P}_n$ (up to a global phase) arises after measurements, where $E_j = I, X, Y$, or Z with equal probability $\frac{1}{4}$ if $j \in \mathfrak{r}$, and $E_j = I$ if $j \in \bar{\mathfrak{r}}$. Although E is unknown, a syndrome $\mathbf{s} = \langle \mathbf{E}, \mathbf{H} \rangle \in \{0, 1\}^{n-k}$ is obtained, where \mathbf{E} and \mathbf{H} are the binary representation of the error and check matrix, respectively.

C. Decoding by solving linear equations

The erasure decoding can be resolved by solving a system of linear equations [28, 34]. We define this decoding by using the notation here. First, express $\langle \mathbf{E}, \mathbf{H} \rangle = \mathbf{s}$ as $\mathbf{E} \mathbf{\Lambda} \mathbf{H}^T = \mathbf{s}$, or equivalently, $(\mathbf{H} \mathbf{\Lambda}) \mathbf{E}^T = \mathbf{s}^T$. Then we have:

Definition 4. For a stabilizer code with a binary check matrix \mathbf{H} , given the erasure information $\mathfrak{r} \subseteq \{1, 2, \dots, n\}$ and syndrome \mathbf{s} , where $\mathbf{s} = \langle \mathbf{E}, \mathbf{H} \rangle$ for some \mathbf{E} drawn from the erasure channel, an erasure decoding by solving a system of linear equations is done by solving

$$\begin{cases} (\mathbf{H}\mathbf{\Lambda})\mathbf{E}^T = [\mathbf{H}^Z | \mathbf{H}^X](\mathbf{E}^X | \mathbf{E}^Z)^T = \mathbf{s}^T, \\ (\mathbf{E}_j^X | \mathbf{E}_j^Z) = (0|0) \quad \forall j \in \bar{\mathfrak{r}}, \end{cases} \quad (7)$$

where $[\mathbf{H}^Z | \mathbf{H}^X]$ is an $(n-k) \times 2n$ binary matrix, $(\mathbf{E}^X | \mathbf{E}^Z)$ contains $2n$ unknown binary variables, and \mathbf{s}^T is known.

Since \mathbf{s} is produced from \mathbf{E} , we always have at least one solution to (7). The information \mathfrak{r} simplifies the problem in (7). For a matrix (or vector) $A = [A_{ij}]$ of $2n$ columns, let $A_{\mathfrak{r}}$ be the submatrix of A restricted to the columns specified by \mathfrak{r} . We simplify the decoding problem in Def. 4 by solving (7) restricted to the erased coordinates \mathfrak{r} :

$$[\mathbf{H}_{\mathfrak{r}}^Z | \mathbf{H}_{\mathfrak{r}}^X](\mathbf{E}_{\mathfrak{r}}^X | \mathbf{E}_{\mathfrak{r}}^Z)^T = \mathbf{s}^T. \quad (8)$$

The code's minimum distance determines whether there is a unique solution to (8). We first define the minimum distance of a stabilizer code [51, 52]. For a Pauli $E \in \mathcal{P}_n$, let its weight $w(E)$ be the number of non-identity components. For its binary form $\mathbf{E} = \varphi(E)$, define the *generalized weight* of \mathbf{E} as $\text{gw}(\mathbf{E}) = w(E)$. Given a stabilizer group $S < \mathcal{P}_n$, its normalizer in \mathcal{P}_n is $\mathcal{N}(S) = \{E \in \mathcal{P}_n : EF = FE \forall F \in S\}$. Recall that $C = \varphi(S) = \text{Row}(\mathbf{H})$, and define $C^\perp = \varphi(\mathcal{N}(S)) = \{\mathbf{v} \in \{0, 1\}^{2n} : \langle \mathbf{v}, \mathbf{H} \rangle = 0\}$. Note that $S < \mathcal{N}(S)$ and $C \subseteq C^\perp$. For $k \geq 1$, the minimum-distance of the stabilizer code is

$$d = \min\{\text{gw}(\mathbf{E}) : \mathbf{E} \in C^\perp \setminus C\}. \quad (9)$$

An $[[n, k]]$ code with minimum distance d is an $[[n, k, d]]$ code. For $k = 0$, we have $C^\perp = C$. The minimum distance in this case is defined as

$$d' = \min\{\text{gw}(\mathbf{E}) : \mathbf{E} \in C^\perp \setminus \mathbf{0}\}. \quad (10)$$

We also define d' for $k \geq 1$. In general, $d' \leq d$. If $d' < d$, the code is a degenerate code. With large $d - d'$, the code has strong degeneracy (or say, the code is highly degenerate). If $d' = d$, the code is called a non-degenerate code, yet it still exhibits some degeneracy, as discussed earlier (4).

Similar to the classical coding theory [61], a non-zero vector \mathbf{E} with $\text{gw}(\mathbf{E}) \leq d' - 1$ always chooses a set of columns in \mathbf{H} that are linearly independent. Notice that in (7), \mathbf{s}^T (a column vector) is generated by columns of $\mathbf{H}\mathbf{\Lambda}$ (which are just columns of \mathbf{H}) using non-zero entries of \mathbf{E} . Thus, if $|\mathfrak{r}| \leq d' - 1$, the columns of $[\mathbf{H}_{\mathfrak{r}}^Z | \mathbf{H}_{\mathfrak{r}}^X]$ in (8) are linearly independent, and hence there is a unique solution $\hat{\mathbf{E}}$ to (8), and the solution is the actual error, i.e., $\hat{\mathbf{E}} = \mathbf{E}$. An MLD always has a successful decoding with $\Pr(\hat{\mathbf{E}} = \mathbf{E}) = 1$ in this case.

If $|\mathfrak{r}| \geq d'$, multiple solutions to (8) exist. We separate this to two cases as follows. First, if $d' \leq |\mathfrak{r}| \leq d - 1$, then all solutions are in the same logical coset containing \mathbf{E} . This

is because an obtained solution $\hat{\mathbf{E}}$ is equivalent to the actual error \mathbf{E} up to a stabilizer, according to (9) and (10). Thus, any solutions $\hat{\mathbf{E}}$ of (7) are in the logical coset of the actual error. An MLD always has a successful decoding with $\Pr(\hat{\mathbf{E}} \in \mathbf{E} + C) = 1$ in this case.

Second, if $|\mathfrak{r}| \geq d$, then some syndromes \mathbf{s} may result in solutions of (8) spanning multiple logical cosets. However, if most syndromes \mathbf{s} do not lead to this case, which happens when physical error rate is no larger than a certain level, we have the advantage that the decoding failure rate is low. For example, this advantage manifests in classical LDPC codes [29, 46], and QLDPC codes [18, 34].

D. A sphere-packing bound for performance evaluation

It is known that a long (Q)LDPC code can correct most errors of weight up to a large t that exceeds the minimum distance [45–47]. We aim to error-correction performance with t proportional to n , establishing a reference for the error threshold. To this end, we derive a sphere-packing bound on the decoding failure probability at an erasure error rate p near a given relative correction radius, t/n .

Consider a channel with erasure probability $p \in (0, 0.5)$. If a qubit is erased, it encounters I, X, Y , or Z with equal probability $1/4$. Using (5) in (6), a qubit encounters I with probability $1 - p + \frac{p}{4} = 1 - \frac{3}{4}p$, and encounters X, Y , or Z with equal probability $\frac{p}{4}$. Thus, before specifying any particular erasure set \mathfrak{r} , the error distribution is given by

$$(p^I, p^X, p^Y, p^Z) = (1 - \frac{3p}{4}, \frac{p}{4}, \frac{p}{4}, \frac{p}{4}). \quad (11)$$

When n and $t \approx np$ are large, we expect errors $E \in \mathcal{P}_n$, with approximately $\frac{3}{4}t$ components being X, Y , or Z . Consequently, we define the logical error rate of *erasure bounded-distance-decoding* (eBDD) with parameters n, t , and p as

$$P_{\text{eBDD}}(n, t, p) := 1 - \sum_{j=0}^{\lceil \frac{3}{4}t \rceil} \binom{n}{j} (\frac{3}{4}p)^j (1 - \frac{3}{4}p)^{n-j}. \quad (12)$$

To bound (12), define the typical BDD error probability $P_{\text{BDD}}(n, t', p') := 1 - \sum_{j=0}^{t'} \binom{n}{j} (p')^j (1 - p')^{n-j}$. Given a fixed ratio $\frac{t'}{n}$ and a small $\varepsilon > 0$, the probability $P_{\text{BDD}}(n, t', p')$ as a function of p' exhibits a sharp decline at $p' = \frac{t'}{n} - \varepsilon$, with exponential decay in n , by a bound from Hoeffding's inequality [62] under the condition $t' \geq np'$:

$$P_{\text{BDD}}(n, t', p') \leq \exp(-2n(\frac{t'}{n} - p')^2) \Big|_{p' = \frac{t'}{n} - \varepsilon} = \exp(-2n\varepsilon^2).$$

Since $P_{\text{eBDD}}(n, t, p) = P_{\text{BDD}}(n, t', p')$ with $t' = \lceil \frac{3}{4}t \rceil$ and $p' = \frac{3}{4}p$, the function $P_{\text{eBDD}}(n, t, p)$ decays exponentially in n at $p = \frac{t}{n} - \frac{4}{3}\varepsilon$ for a fixed ratio $\frac{t}{n}$ and small $\varepsilon > 0$.

Proposition 1. If a family of codes has performance closely matching $P_{\text{eBDD}}(n, t, p)$ (12) at a specific $\frac{t}{n} = p_{\text{th}}$ as n grows, then this p_{th} serves an estimated threshold for the code family.

III. COSET STRUCTURE OF STABILIZER CODES AND MAXIMUM-LIKELIHOOD DECODING

In this section, paralleling [37, Lemma 1], we present Theorem 4, drawing on group theory and probability theory. The theorem states that any erasure- and syndrome-matched solution (termed a *feasible* solution for (7)) is an optimal solution for QMLD in Def. 2. To clarify this erasure decoding scenario for stabilizer codes, we provide a specific example (see Example 1 and Fig. 1).

A. Coset structure of stabilizer codes

The generators of $\mathcal{N}(\mathcal{S})$, which contains \mathcal{S} , have a simple representation [58, Sec. 4]. Using elementary row operations on the matrix (3) (together with equivalent transformations $X \leftrightarrow Z$ [51] used on selected qubits [58]), we obtain a standard form [58, 63] of the binary check matrix

$$\mathbf{H} = \left[\mathbf{1}_{n-k} \quad \mathbf{A} \mid \mathbf{B} \quad \mathbf{C} \right], \quad (13)$$

where $\mathbf{A}, \mathbf{C} \in \{0, 1\}^{(n-k) \times k}$ and $\mathbf{B} \in \{0, 1\}^{(n-k) \times (n-k)}$. To find the null space of \mathbf{H} , we construct a full row-rank $(n+k) \times 2n$ binary matrix \mathbf{G} by adding $2k$ rows to (13):

$$\mathbf{G} = \left[\begin{array}{cc|cc} \mathbf{1}_{n-k} & \mathbf{A} & \mathbf{B} & \mathbf{C} \\ \mathbf{0} & \mathbf{1}_k & \mathbf{C}^T & \mathbf{0} \\ \mathbf{0} & \mathbf{0} & \mathbf{A}^T & \mathbf{1}_k \end{array} \right] = \left[\begin{array}{c} \mathbf{H} \\ \mathbf{L} \end{array} \right]. \quad (14)$$

It is easy to verify that \mathbf{G} has full row-rank and satisfies $\langle \mathbf{G}, \mathbf{H} \rangle = \mathbf{G} \mathbf{A} \mathbf{H}^T = \mathbf{0}$. Hence, the rows of \mathbf{G} are binary representations of generators of $\mathcal{N}(\mathcal{S})$. Let C^\perp be the dual code of C with respect to the symplectic inner product. Then C^\perp is the row-space of \mathbf{G} , and we have

$$\varphi(\mathcal{N}(\mathcal{S})) = C^\perp = \text{Row}(\mathbf{G}).$$

By further adding $n-k$ binary vectors of length $2n$ to (14), we form a $2n \times 2n$ matrix

$$\left[\begin{array}{cc|cc} \mathbf{1}_{n-k} & \mathbf{A} & \mathbf{B} & \mathbf{C} \\ \mathbf{0} & \mathbf{1}_k & \mathbf{C}^T & \mathbf{0} \\ \mathbf{0} & \mathbf{0} & \mathbf{A}^T & \mathbf{1}_k \\ \mathbf{0} & \mathbf{0} & \mathbf{1}_{n-k} & \mathbf{0} \end{array} \right] = \left[\begin{array}{c} \mathbf{H} \\ \mathbf{L} \\ \mathbf{V} \end{array} \right] = \left[\begin{array}{c} \mathbf{G} \\ \mathbf{V} \end{array} \right]. \quad (15)$$

The rows in the matrix (15) span the vector space $\{0, 1\}^{2n}$.

Note the following coset structure. Observe that

$$C = \text{Row}(\mathbf{H}) \subseteq \text{Row}(\mathbf{G}) = C^\perp \subseteq \{0, 1\}^{2n}. \quad (16)$$

Together with (15), we have the following quotient group:

$$\{0, 1\}^{2n} / C^\perp = \{\mathbf{v} + C^\perp : \mathbf{v} \in \text{Row}(\mathbf{V})\}.$$

This partitions $\{0, 1\}^{2n}$ into 2^{n-k} non-overlapping *error cosets*, and each coset contains $|C^\perp| = 2^{n+k}$ vectors sharing the same syndrome. Distinct error cosets are identified by distinct error coset leaders in $\{\mathbf{v}^{(i)}\}_{i=1}^{2^{n-k}} = \text{Row}(\mathbf{V})$.

Similarly, by (16), together with (14), we have another quotient group:

$$C^\perp / C = \{\ell + C : \ell \in \text{Row}(\mathbf{L})\}. \quad (17)$$

This partitions C^\perp into 2^{2k} non-overlapping logical cosets, and each logical coset contains $|C| = 2^{n-k}$ vectors. Distinct logical cosets in (17) are identified by distinct logical coset leaders in $\{\ell^{(j)}\}_{j=1}^{2^{2k}} = \text{Row}(\mathbf{L})$, where \mathbf{L} is in (14) or (15).

Like the classical standard array for decoding [61], we construct a quantum standard array for decoding [58]:

$$\left[\begin{array}{cccc} \mathbf{v}^{(1)} + \ell^{(1)} + C & \mathbf{v}^{(1)} + \ell^{(2)} + C & \dots & \mathbf{v}^{(1)} + \ell^{(2^{2k})} + C \\ \mathbf{v}^{(2)} + \ell^{(1)} + C & \mathbf{v}^{(2)} + \ell^{(2)} + C & \dots & \mathbf{v}^{(2)} + \ell^{(2^{2k})} + C \\ \vdots & \vdots & \ddots & \vdots \\ \mathbf{v}^{(2^{n-k})} + \ell^{(1)} + C & \mathbf{v}^{(2^{n-k})} + \ell^{(2)} + C & \dots & \mathbf{v}^{(2^{n-k})} + \ell^{(2^{2k})} + C \end{array} \right]. \quad (18)$$

In (18), there are 2^{n-k} rows, each representing an error coset with the same syndrome, and every row contains 2^{2k} logical cosets. (Examples are shown in Fig. 1.)

We introduce some notation used in the following. Consider a stabilizer code with a binary check matrix \mathbf{H} , and let $E \in \mathcal{P}_n$ be a Pauli error with binary representation $\varphi(E) = \mathbf{E}$ and syndrome $\mathbf{s}(E) = \langle \mathbf{E}, \mathbf{H} \rangle$. The error E is in some coset $\mathbf{v}^{(i)} + \ell^{(j)} + C$ located in (18). We denote these $\mathbf{v}^{(i)}$ and $\ell^{(j)}$ by $\mathbf{v}^{(\mathbf{s}(E))}$ and $\ell^{(E)}$, respectively.

Note that $\mathbf{v}^{(\mathbf{s}(E))} = (\mathbf{0}, \mathbf{0} \mid \mathbf{s}, \mathbf{0})$ when \mathbf{H} is in the standard form (13). However, calculating $\ell^{(E)}$ is non-trivial.

B. Maximum-likelihood decoding

Consider a stabilizer code with $\varphi(\mathcal{S}) = C \subseteq \{0, 1\}^{2n}$. In MLD, one aims to find an error estimate \hat{E} in a logical coset $\mathbf{v}^{(\mathbf{s}(E))} + \ell^{(E)} + C$ such that the sum of the probabilities of elements in the logical coset is maximized compared to other logical cosets, given the erasure information $\mathfrak{r} \subseteq \{1, 2, \dots, n\}$ and syndrome $\mathbf{s} \in \{0, 1\}^{n-k}$.

Given a $p \in (0, 0.5)$, the probability to obtain an erasure pattern \mathfrak{r} is

$$\Pr(\mathfrak{r}) = p^{|\mathfrak{r}|} (1-p)^{n-|\mathfrak{r}|}. \quad (19)$$

For an $E \in \{0, 1\}^{2n}$ (with corresponding $E \in \mathcal{P}_n$), according to the erasure channel model, we have the conditional probability of E given \mathfrak{r}

$$\Pr(E \mid \mathfrak{r}) = \begin{cases} (1/4)^{|\mathfrak{r}|}, & \text{if } E_j = I \ \forall j \in \bar{\mathfrak{r}}, \\ 0, & \text{otherwise.} \end{cases} \quad (20)$$

By Bayes' rule, the conditional probability of E given a certain \mathfrak{r} and \mathbf{s} is

$$\Pr(E \mid \mathfrak{r}, \mathbf{s}) = \frac{\Pr(E) \Pr(\mathfrak{r}, \mathbf{s} \mid E)}{\Pr(\mathfrak{r}, \mathbf{s})}. \quad (21)$$

We have $\Pr(\mathfrak{r}, \mathbf{s}) > 0$ since the syndrome is produced from the erasure error, and it is a constant. The numerator in

(21) is either a constant or 0; to see this, rewrite (21) as

$$\Pr(\mathbf{E} | \mathfrak{r}, \mathbf{s}) = \frac{\Pr(\mathbf{E}, \mathfrak{r}, \mathbf{s})}{\Pr(\mathfrak{r}, \mathbf{s})} = \frac{\Pr(\mathfrak{r}) \Pr(\mathbf{E} | \mathfrak{r}) \Pr(\mathbf{s} | \mathbf{E}, \mathfrak{r})}{\Pr(\mathfrak{r}, \mathbf{s})}. \quad (22)$$

The term $\Pr(\mathfrak{r})$ is a constant as in (19). The term $\Pr(\mathbf{E} | \mathfrak{r})$ is either a constant or 0 as in (20). The term $\Pr(\mathbf{s} | \mathbf{E}, \mathfrak{r})$ is either 1 or 0, depending on whether \mathbf{E} is an erasure- and syndrome-matched error or not. Such an \mathbf{E} has $\Pr(\mathfrak{r}, \mathbf{s} | \mathbf{E}) \neq 0$ and is a feasible solution for (7).

Consequently, we represent (21) as

$$\Pr(\mathbf{E} | \mathfrak{r}, \mathbf{s}) = \begin{cases} \text{a constant} \propto (1/4)^{|\mathfrak{r}|}, & \text{if } \Pr(\mathfrak{r}, \mathbf{s} | \mathbf{E}) \neq 0, \\ 0, & \text{otherwise.} \end{cases} \quad (23)$$

The CMLD in Def. 1 aims to maximize (21). However, all erasure- and syndrome-matched errors—which are all feasible solutions to (7)—are equally good solutions, as demonstrated in (23). This leads to:

Lemma 2. *For a stabilizer code with $\varphi(S) = C \subset \{0, 1\}^{2n}$, if erasures $\mathfrak{r} \subseteq \{0, 1, \dots, n\}$ and syndrome $\mathbf{s} \in \{0, 1\}^{n-k}$ are given for decoding, then any erasure and syndrome-matched $\mathbf{E} \in \{0, 1\}^{2n}$, which is a feasible solution to (7), is an optimal solution for CMLD as defined in Def. 1.*

In contrast, QMLD in Def. 2 aims to maximize the following conditional probability of a logical coset given \mathfrak{r} and \mathbf{s}

$$\Pr(\mathbf{E} + C | \mathfrak{r}, \mathbf{s}) := \sum_{\mathbf{E}' \in \mathbf{E} + C} \Pr(\mathbf{E}' | \mathfrak{r}, \mathbf{s}), \quad (24)$$

where $\Pr(\mathbf{E}' | \mathfrak{r}, \mathbf{s})$ is either a positive constant or 0 by (23). Also, a positive $\Pr(\mathbf{E}' | \mathfrak{r}, \mathbf{s})$ has \mathbf{E}' as an erasure- and syndrome-matched error, as in (23). Consequently, a maximum likelihood coset is a coset with the most number of erasure- and syndrome-matched errors. Next, we prove:

Lemma 3. *If two distinct logical cosets both contain erasure- and syndrome-matched errors, then the number of such errors in both cosets is equal, and they both are maximum likelihood logical cosets.*

Proof. Let $\mathfrak{r} \subseteq \{1, 2, \dots, n\}$ and $\mathbf{s} \in \{0, 1\}^{n-k}$ denote the erasure information and the syndrome, respectively. Let $\mathbf{E}, \mathbf{F} \in \{0, 1\}^{2n}$ be two erasure- and syndrome-matched errors in different logical cosets $\mathbf{E} + C \neq \mathbf{F} + C$. Let

$$\{\tilde{\mathbf{E}}\} := \{\mathbf{E}' \in \mathbf{E} + C : (\mathbf{E}'^X | \mathbf{E}'^Z) = (0|0) \forall j \in \bar{\mathfrak{r}}\},$$

which contains degenerate errors of \mathbf{E} that are also erasure-matched. We represent

$$\begin{aligned} \{\tilde{\mathbf{E}}\} &\subseteq \mathbf{E} + C = \mathbf{v}^{(s(\mathbf{E}))} + \boldsymbol{\ell}^{(\mathbf{E})} + C, \text{ and} \\ \{\tilde{\mathbf{F}}\} &\subseteq \mathbf{F} + C = \mathbf{v}^{(s(\mathbf{F}))} + \boldsymbol{\ell}^{(\mathbf{F})} + C, \end{aligned}$$

where the equalities are by the notation after (18). We have $\Pr(\mathbf{E} + C | \mathfrak{r}, \mathbf{s}) \propto |\{\tilde{\mathbf{E}}\}|$ and $\Pr(\mathbf{F} + C | \mathfrak{r}, \mathbf{s}) \propto |\{\tilde{\mathbf{F}}\}|$ as in the discussion for (24). For this lemma, it suffices to show that $|\{\tilde{\mathbf{E}}\}| = |\{\tilde{\mathbf{F}}\}|$. Using the above representation and the

assumption $\mathbf{s}(\mathbf{E}) = \mathbf{s}(\mathbf{F})$, we have that $\mathbf{E} + C$ and $\mathbf{F} + C$ differ by a vector $\boldsymbol{\ell}' = \boldsymbol{\ell}^{(\mathbf{E})} - \boldsymbol{\ell}^{(\mathbf{F})} \in \text{Row}(\mathbf{L})$, where \mathbf{L} is in (15). For our purpose, we choose a difference vector $\boldsymbol{\ell} = \mathbf{E} - \mathbf{F}$, which is not necessarily equal to $\boldsymbol{\ell}'$ but differs by a stabilizer, i.e., $\boldsymbol{\ell} - \boldsymbol{\ell}' \in C$. By our choice of $\boldsymbol{\ell}$, we have $(\boldsymbol{\ell}_j^X | \boldsymbol{\ell}_j^Z) = (0|0)$ for all $j \in \bar{\mathfrak{r}}$. With $\boldsymbol{\ell}$ as a mapping, the elements in $\{\tilde{\mathbf{E}}\}$ are in one-to-one correspondence with the elements in $\{\tilde{\mathbf{F}}\}$. Thus, $|\{\tilde{\mathbf{E}}\}| = |\{\tilde{\mathbf{F}}\}|$. \square

A consequence of Lemma 3 is that any logical coset containing an erasure- and syndrome-matched solution is a maximum likelihood logical coset. Thus, we have:

Theorem 4. *For a stabilizer code with $\varphi(S) = C \subset \{0, 1\}^{2n}$, if erasures $\mathfrak{r} \subseteq \{1, 2, \dots, n\}$ and syndrome $\mathbf{s} \in \{0, 1\}^{n-k}$ are given for decoding, then any erasure and syndrome-matched $\mathbf{E} \in \{0, 1\}^{2n}$, which is a feasible solution to (7), is an optimal solution for QMLD in Def. 2.*

Example 1. Consider a $[[4, 1]]$ code with this check matrix

$$\mathbf{H} = [\mathbf{H}^X | \mathbf{H}^Z] = \begin{bmatrix} 1 & 0 & 0 & 0 & | & 0 & 0 & 1 & 0 \\ 0 & 1 & 0 & 1 & | & 0 & 1 & 0 & 1 \\ 0 & 0 & 1 & 1 & | & 1 & 0 & 0 & 1 \end{bmatrix}, \quad (25)$$

or equivalently, its Pauli check matrix

$$\mathbf{H} = \begin{bmatrix} X & I & Z & I \\ I & Y & I & Y \\ Z & I & X & Y \end{bmatrix}. \quad (26)$$

Given a syndrome, there are $2^{2k} = 4$ logical cosets. When syndrome $\mathbf{s} = (0|10)$, the corresponding four logical cosets in Pauli form are:

$$\begin{bmatrix} I & Z & I & I & \leftarrow \\ X & Z & Z & I & \leftarrow \\ I & X & I & Y & \leftarrow \\ X & X & Z & Y & \\ Z & Z & X & Y & \\ Z & Z & Y & Y & \\ Z & X & X & I & \\ Y & X & Y & I & \end{bmatrix}, \quad \begin{bmatrix} I & I & Z & X \\ X & I & I & X \\ I & Y & Z & Z \\ X & Y & I & Z \\ Y & I & Y & Z \\ Y & I & X & Z \\ Z & Y & Y & X \\ Y & Y & X & X \end{bmatrix}, \quad \begin{bmatrix} I & I & Z & Z \\ X & I & I & Z \\ I & Y & Z & X \\ X & Y & I & X \\ Z & I & Y & X \\ Y & I & X & X \\ Z & Y & Y & Z \\ Y & Y & X & Z \end{bmatrix}, \quad \begin{bmatrix} I & Z & I & Y & \leftarrow \\ X & Z & Z & Y & \leftarrow \\ I & X & I & I & \leftarrow \\ X & X & Z & I & \\ Z & Z & X & I & \\ Y & Z & Y & I & \\ Z & X & X & Y & \\ Y & X & Y & Y & \end{bmatrix},$$

where left arrows indicate the errors to be discussed.

When only the second qubit is erased, we easily identify a unique solution $IZII$. We show this case in Fig. 1(a).

When the 2nd and 4th qubits are erased, i.e., $\mathfrak{r} = \{2, 4\}$, we have $E_j = I$ for $j \in \bar{\mathfrak{r}} = \{1, 3\}$. As indicated by the left arrows above, the occurred error is a Pauli operator in either

$$\begin{bmatrix} I & Z & I & I \\ I & X & I & Y \end{bmatrix} \quad \text{or} \quad \begin{bmatrix} I & Z & I & Y \\ I & X & I & I \end{bmatrix}. \quad (27)$$

The two sets in (27) differ by a difference $IIIIY$, which have identity at qubit $j \in \bar{\mathfrak{r}} = \{1, 3\}$. We show this case in Fig. 1(b).

A decoder can fail in two ways: either it fails to converge to the given syndrome, or it converges to an incorrect logical coset. An MLD fails only in the second way. Both types of failures result in a logical error, occurring with probability $\Pr(\hat{\mathbf{E}} \notin \mathbf{E} + C)$, called *logical error rate*. The second type of failure, known as false convergence, has probability $\Pr(\langle \hat{\mathbf{E}}, \mathbf{H} \rangle = \mathbf{s}, \hat{\mathbf{E}} \notin \mathbf{E} + C)$, called *false convergence rate*.

Lemma 5. *A decoder is an MLD if and only if it always finds a feasible solution to (7). Equivalently, a decoder is an MLD if and only if it exhibits identical logical error and false convergence rates.*

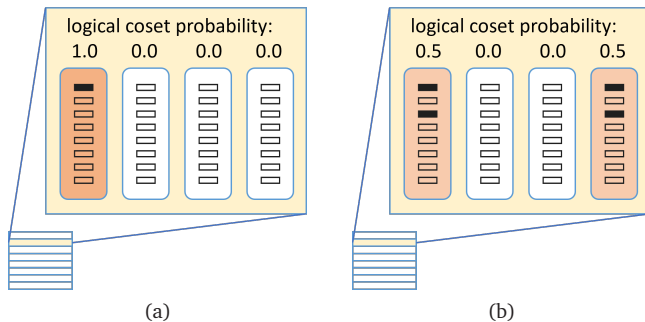


FIG. 1: Coset structure and logical coset probability for the $[[4, 1]]$ code in Example 1, given syndrome $\mathbf{s} = (0, 1, 0)$ and erasures (a) $\mathfrak{r} = \{2\}$ or (b) $\mathfrak{r} = \{2, 4\}$. An MLD identifies an error in any logical coset with positive probability. Uniqueness of the solution depends on code distance and erasure count $|\mathfrak{r}|$. The structure here follows the quantum standard array (18).^a

^a Each subfigure shows $2^{n-k} = 8$ error cosets, with the highlighted one (the 2nd row) matching the syndrome $\mathbf{s} = (0, 1, 0)$. Every coset contains $2^{2k} = 4$ logical cosets, each with $2^{n-k} = 8$ errors. Errors are depicted as bars, with positive-probability errors (which have equal probability) shown in black.

Corollary 6. *A decoder with approximately equal logical error and false convergence rates performs closely to MLD. Furthermore, the decoder's false convergence rate provides a useful lower bound on the logical error rate achievable by MLD.*

For long codes, decoding via Gaussian elimination as a reference for MLD is often impractical. Lemma 5 and Corollary 6 provide a useful criterion for assessing whether a decoder achieves or approximates MLD performance.

IV. BELIEF PROPAGATION ALGORITHMS

Here, we propose decoding algorithms based on BP. This decoding strategy, first introduced for classical codes, is known as the sum-product algorithm [46], and is usually understood as Pearl's BP [47, 64], which runs an iterative messaging-passing on a Tanner graph [65, 66].

For erasure decoding, it is generally sufficient to use the matrix \mathbf{H} instead of $\mathbf{H}\mathbf{\Lambda} = [\mathbf{H}^Z | \mathbf{H}^X]$. Accordingly, we may sometimes do so in the following to simplify notation.

A Tanner graph induced by an $m \times 2n$ binary check matrix \mathbf{H} is a bipartite graph consisting of m check nodes and $2n$ binary variable nodes. An edge connects check node i and variable node j if $\mathbf{H}_{ij} = 1$. Also, when $\mathbf{H}_{ij} = 1$, we say that row i checks column j .

On the other hand, a (quaternary) Tanner graph induced by an $m \times n$ Pauli check matrix H is similarly defined, with extended edge types $H_{ij} \in \{X, Y, Z\}$. Given a code, its binary check matrix and Pauli check matrix induce different Tanner graphs.

Example 2. *The binary check matrix (25) has a Tanner graph in Fig. 2(a). The corresponding Pauli check matrix (26) has a Tanner graph in Fig. 2(b).*

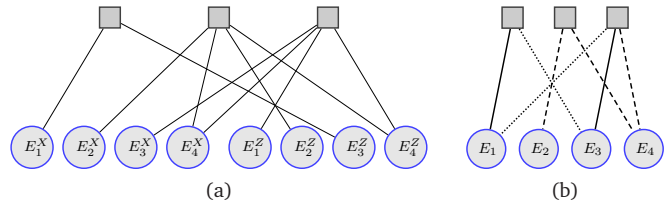


FIG. 2: (a) The Tanner graph induced by the binary check matrix in (25). (b) The Tanner graph induced by the Pauli check matrix in (26), with edge types X, Y, Z , indicated by solid, dashed, and dotted lines, respectively.

We define the concept of stopping sets by considering the binary check matrix \mathbf{H} of a code $C = \varphi(\mathcal{S})$.

Definition 5. (*Stopping sets*) [29, 31–33, 35, 36] *Let $ST \subseteq \{1, \dots, 2n\}$. The subset ST is a stopping set of a binary check matrix \mathbf{H} if, for every row of \mathbf{H} , the row either checks no variable from ST or checks at least two variables from ST .*

When a stabilizer code of length n is described as a binary code of length $2n$, the quantum erasure decoding problem (cf. Def. 4) is like a classical erasure decoding problem [28, 34]. For efficiency, Flip-BP₂ is usually conducted for decoding, which passes messages on a Tanner graph like Fig. 2(a) [28–33]. This decoder performs iterative *bit-flipping* to flip unknown bits in (7) to find a feasible solution. In Flip-BP₂, a bit is chosen to flip if it is a single unknown variable (bit) in a check. However, Flip-BP₂ may easily terminate earlier before finding a feasible solution, if the code contains small stopping sets [29–33, 35, 36]. This prevents the decoder from converging.

Example 3. *Consider the binary \mathbf{H} in (25), which induces a Tanner graph in Fig. 2(a). Variable coordinates corresponding to E_4^X and E_4^Z form a stopping set. If the fourth qubit is erased ($\mathfrak{r} = \{4\}$) and $E = I \otimes I \otimes I \otimes Y$, then Flip-BP₂ stops before finding a feasible solution. The matrix \mathbf{H} restricted to $\mathfrak{r} = \{4\}$ is $[\mathbf{H}_{\mathfrak{r}}^X | \mathbf{H}_{\mathfrak{r}}^Z] = \begin{bmatrix} 0 & 0 \\ 1 & 1 \\ 1 & 1 \end{bmatrix}$.*

The length of the shortest cycle in a graph is called *girth*. The size of the smallest stopping set of a code is called *stopping number*. We discuss the results from [36]:

Remark 7. *For codes with binary \mathbf{H} of constant column-weight at least 3, the stopping number σ increases with the girth g as follows: $\sigma = 2$ for $g = 4$, $\sigma = d + 1$ for $g = 6$, $\sigma = 2d$ for $g = 8$, and σ grows exponentially with g for $g > 8$.*

Remark 8. *The stopping number lower bounds the classical minimum distance of the code. Thus, a small classical minimum distance imposes a small stopping number¹.*

¹ This is not shown in [36] but follows from Sec. II C. A small classical minimum distance implies a small set of linearly dependent columns in \mathbf{H} . When \mathfrak{r} matches this set, (8) lacks a unique solution, causing BP to stop earlier. Thus, this set leads to a small stopping number.

Example 4. In Example 3, the restricted matrix $[\mathbf{H}_r^X | \mathbf{H}_r^Z]$ has a submatrix $\begin{bmatrix} 1 & 1 \\ 1 & 1 \end{bmatrix}$, which forms a four-cycle in the Tanner graph. A four-cycle is a cycle of shortest length. By treating \mathbf{H} in (25) as a parity-check matrix of a classical code of length 8, the code has small girth 4. Note that the code has a classical minimum distance 2, and its stopping number is 2.

It is possible to construct QLDPC codes with favourable girth properties (cf. Sec. VC), but preventing small stopping sets is not possible. For stabilizer codes, we have $C = \text{Row}(\mathbf{H}) \subseteq \text{Row}(\mathbf{G}) = C^\perp$. A QLDPC code typically contains numerous small-weight classical codewords in C^\perp due to the low density of \mathbf{H} , which introduces many small stopping sets (Remark 8). This leads to the following dilemma:

Remark 9. We aim for a QLDPC code with a binary check matrix \mathbf{H} as sparse as possible; however, the code's stopping number is upper bounded by the minimum row-weight of \mathbf{H} .

Sparsity is crucial for low-complexity system implementation and decoding. We seek a decoder with strong convergence that is not adversely affected by small stopping sets, rather than increasing sparsity during code construction. In the following, we propose our algorithms.

A. Gradient-descent based Flipping BP

When Flip-BP₂ stops before finding a feasible solution $\hat{\mathbf{E}}$ for (7), we set an unresolved bit in $\hat{\mathbf{E}}$ to 1 so that the sum of the numbers of unresolved bits, observed from each check, is minimum. This is like a gradient-descent (GD). We propose a GD Flip-BP₂, as stated in Algorithm 1. Note that, without loss of generality, we state input \mathbf{H} instead of $\mathbf{H}\mathbf{\Lambda}$ (see (7)). The algorithm is explained as follows.

Since the binary check matrix have $2n$ columns, we have the set of erased coordinates $\mathfrak{r}_2 \subseteq \{1, 2, \dots, 2n\}$. When we simulate quantum erasures, i.e., when having an $\mathfrak{r} \subseteq \{1, 2, \dots, n\}$, we set $\mathfrak{r}_2 = \mathfrak{r} \cup (\mathfrak{r} + n)$, where $\mathfrak{r} + n = \{j + n : j \in \mathfrak{r}\}$. In general, a check matrix has $m \geq n - k$ rows. For a binary check matrix \mathbf{H} , check node i has neighbouring variable nodes with indices in the set

$$\mathcal{N}(i) = \{j \in \{1, 2, \dots, 2n\} : \mathbf{H}_{ij} = 1\}, \quad (28)$$

and variable node j has neighbouring check nodes with indices in the set

$$\mathcal{M}(j) = \{i \in \{1, 2, \dots, m\} : \mathbf{H}_{ij} = 1\}. \quad (29)$$

The computation proceeds by mapping $\{0, 1\} \rightarrow \{+1, -1\}$ and ERASE $\mapsto 0$. Every variable node has its own belief $\Gamma_j \in \{-1, 0, +1\}$ to be updated by message-passing. Every check node has a local message Δ_i , storing the number of unresolved bits observed from this check. Variable-to-check messages are represented by $\Gamma_{j \rightarrow i}$, which equals Γ_j in erasure decoding but are created independently in Algorithm 1 to enable parallelism (avoiding the need to race for access to Γ_j in the horizontal step). Check-to-variable messages are represented by $\Delta_{i \rightarrow j}$. For check matrices with bounded

Algorithm 1 : GD Flip-BP₂

Input:

A binary check matrix $\mathbf{H} \in \{0, 1\}^{m \times 2n}$, a syndrome $\mathbf{s} \in \{0, 1\}^m$, erased coordinates $\mathfrak{r}_2 \subseteq \{1, 2, \dots, 2n\}$, and an integer $T_{\max} > 0$.

Initialization.

- Let $\Gamma_j = 0$ if $j \in \mathfrak{r}_2$, and $\Gamma_j = +1$ if $j \in \bar{\mathfrak{r}}_2$.
- For $j \in \{1, 2, \dots, 2n\}$ and $i \in \mathcal{M}(j)$: Let $\Gamma_{j \rightarrow i} = \Gamma_j$.

Horizontal Step.

- Let $\Delta_i = |\mathcal{N}(i) \cap \mathfrak{r}_2|$ for $i = \{1, 2, \dots, m\}$.
- For $i \in \{1, 2, \dots, m\}$ such that $\Delta_i > 0$: for $j \in \mathcal{N}(i) \cap \mathfrak{r}_2$, let

$$\Delta_{i \rightarrow j} = (-1)^{s_i} \prod_{j' \in \mathcal{N}(i) \setminus \{j\}} \Gamma_{j' \rightarrow i}.$$

Vertical Step.

- For $j \in \mathfrak{r}_2$: If any $\Delta_{i \rightarrow j} \neq 0$, where $i \in \mathcal{M}(j)$, update $\Gamma_j = \Delta_{i \rightarrow j}$.
- (GD Step) If no Γ_j is updated in the previous sub-step: Find a $j \in \mathfrak{r}_2$ such that the corresponding column in \mathbf{H} has a maximum column weight. Set $\Gamma_j = -1$.
- For indices j such that Γ_j was updated in this iteration: update $\Gamma_{j \rightarrow i} = \Gamma_j$ for $i \in \mathcal{M}(j)$, and remove j from \mathfrak{r}_2 .

Judgement.

- If $\mathfrak{r}_2 = \emptyset$: set $\hat{\mathbf{E}} \in \{0, 1\}^{2n}$ such that $\hat{E}_j = 0$ if $\Gamma_j = +1$, and $\hat{E}_j = 0$ if otherwise.
 - if $\langle \hat{\mathbf{E}}, \mathbf{H} \rangle = \mathbf{s}$: return “CONVERGE”;
 - else: return “GD_FAIL”.
 - Else: if the maximum number of iterations T_{\max} is reached, halt and return “FAIL”.
 - Repeat from the Horizontal Step.
-

column weights, as is the case for the QLDPC codes we consider, the algorithm has linear complexity $O(n)$ per iteration. While the algorithm can be restricted to the erased coordinates \mathfrak{r}_2 like (8), the per-iteration complexity remains $O(n)$ because on average $|\mathfrak{r}_2| \propto np \propto n$ given p .

It is clear that we can effectively decide a specific Γ_j in Algorithm 1 only if there is a non-zero $\Delta_{i \rightarrow j}$ incoming to variable node $j \in \mathfrak{r}_2$. The GD step is performed when no effective updates occur during an iteration. This step considers an objective function defined as the sum of the numbers of unresolved bits in each check, expressed as

$$\sum_{i=1}^m |\mathcal{N}(i) \cap \mathfrak{r}_2|. \quad (30)$$

We decide which bit to resolve in order to minimize the objective function (30). Naturally, this is the bit with index $j \in \mathfrak{r}_2$ that maximizes the corresponding column weight in \mathbf{H} . We can set the corresponding Γ_j to either $+1$ or -1 ; we choose to set it to -1 (setting the corresponding bit to 1) for simplicity. This simplicity relies on the strong symmetry of degenerate solutions [44].

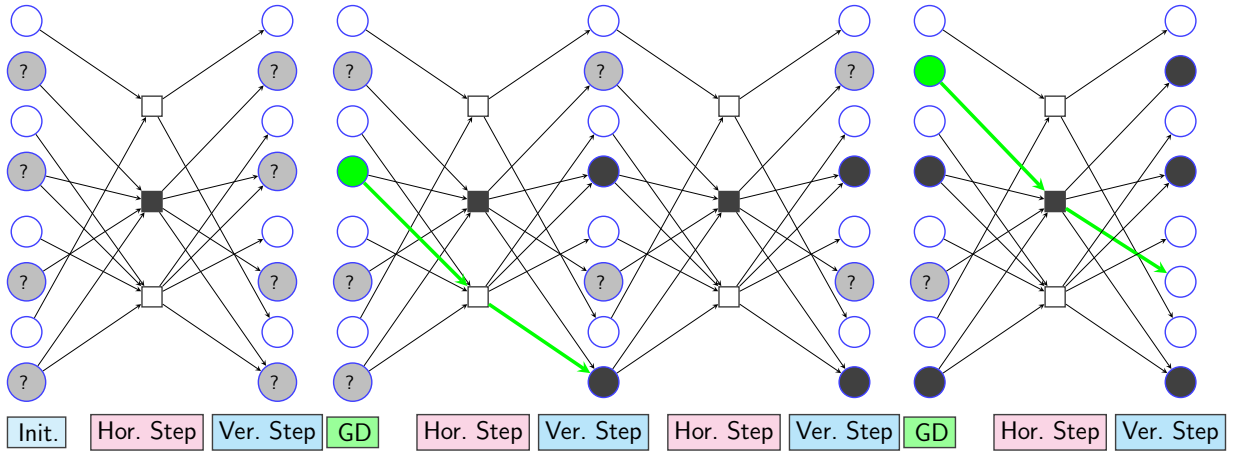


FIG. 3: (coloured online) The decoding process of GD Flip-BP₂ using the binary \mathbf{H} in Example 1 with syndrome $\mathbf{s} = (010)$ and erasures $\mathfrak{r} = \{2, 4\}$, i.e., $\mathfrak{r}_2 = \{2, 4, 6, 8\}$. In the Initialization (Init.), bits 1,3,5,7 are set to 0 (white colour), and bits 2,4,6,8 are set to unknown (with question mark (?)). We present Algorithm 1, which includes Horizontal Step (Hor. Step) and Vertical Step (Ver. Step), as shown in the figure. The 1st iteration has no effective update, so performs GD to set bit 4 to 1 (green colour). This information (green colour) is propagated to correct bit 8 in the 2nd iteration. (Bits with value 1 are with black colour.) The 3rd iteration has no effective update, so performs GD to set bit 2 to 1. This information is propagated to correct bit 6 in the 4th iteration, which resolves all bits. The decoder output is $(0101|0001)$. This is *IXIY* in Pauli notation, which is an erasure- and syndrome-matched solution.

Example 5. For a simple case, consider the binary matrix \mathbf{H} in Example 1, with $\mathfrak{r} = \{4\}$ as in Example 3. Specifically, we have $[\mathbf{H}_{\mathfrak{r}}^X | \mathbf{H}_{\mathfrak{r}}^Z] = \begin{bmatrix} 0 & 0 \\ 1 & 1 \end{bmatrix}$. The syndrome is the column combination of this matrix and can only be either $\mathbf{s}^T = \begin{bmatrix} 0 \\ 0 \end{bmatrix}$ or $\mathbf{s}^T = \begin{bmatrix} 0 \\ 1 \end{bmatrix}$. We are to solve the system of linear equations in Def. 4 or $[\mathbf{H}_{\mathfrak{r}}^Z | \mathbf{H}_{\mathfrak{r}}^X](\mathbf{E}_{\mathfrak{r}}^X | \mathbf{E}_{\mathfrak{r}}^Z)^T = \mathbf{s}^T$ in (8). The feasible solutions for $(\mathbf{E}_{\mathfrak{r}}^X | \mathbf{E}_{\mathfrak{r}}^Z)$ on the 4th qubit are symmetric as follows:

- If $\mathbf{s}^T = \begin{bmatrix} 0 \\ 0 \end{bmatrix}$, we have $(\mathbf{E}_{\mathfrak{r}}^X | \mathbf{E}_{\mathfrak{r}}^Z) = (0|0)$ or $(1|1)$.
- If $\mathbf{s}^T = \begin{bmatrix} 0 \\ 1 \end{bmatrix}$, we have $(\mathbf{E}_{\mathfrak{r}}^X | \mathbf{E}_{\mathfrak{r}}^Z) = (1|0)$ or $(0|1)$.

The solution is not unique so a bit-flipping decoder stops. The GD step will simply set the first bit of $(\mathbf{E}_{\mathfrak{r}}^X | \mathbf{E}_{\mathfrak{r}}^Z)$ to 1. Then in a subsequent iteration:

- If $\mathbf{s}^T = \begin{bmatrix} 0 \\ 0 \end{bmatrix}$, we obtain $(\mathbf{E}_{\mathfrak{r}}^X | \mathbf{E}_{\mathfrak{r}}^Z) = (1|1)$.
- If $\mathbf{s}^T = \begin{bmatrix} 0 \\ 1 \end{bmatrix}$, we obtain $(\mathbf{E}_{\mathfrak{r}}^X | \mathbf{E}_{\mathfrak{r}}^Z) = (1|0)$.

With our proposed GD, the decoder converges in either case.

Example 6. Continuing from Example 5, we consider a larger stopping set by taking $\mathfrak{r} = \{2, 4\}$ with syndrome $\mathbf{s} = (010)$ as in Example 1. Restricted to $\mathfrak{r} = \{2, 4\}$, i.e., $\mathfrak{r}_2 = \{2, 4, 6, 8\}$, we have $\mathbf{H}_{\mathfrak{r}_2} = [\mathbf{H}_{\mathfrak{r}_2}^X | \mathbf{H}_{\mathfrak{r}_2}^Z] = \begin{bmatrix} 0 & 0 & 0 & 0 \\ 1 & 1 & 1 & 1 \\ 0 & 1 & 1 & 0 \end{bmatrix}$. The procedure of Algorithm 1 is illustrated in Fig. 3 to facilitate the understand of our GD Flip-BP₂ algorithm. The decoder converges and outputs *IXIY*. Another solution, with symmetry at qubit 2, is *IZIY*. Further, with the symmetry at qubit 4, two additional solutions are *IXII* and *IZII*, as suggested in (27).

Algorithm 2 : GD Flip-BP₂ (simplified)

Input: The same as in Algorithm 1.

Initialization. Do the same as in Algorithm 1.

Iterative Update.

- For $i \in \{1, 2, \dots, m\}$: Update $\Delta_i = |\mathcal{N}(i) \cap \mathfrak{r}_2|$; Then if $|\mathcal{N}(i) \cap \mathfrak{r}_2| = 1$, let j be the single element in $\mathcal{N}(i) \cap \mathfrak{r}_2$ and set

$$\Gamma_j = (-1)^{s_i} \prod_{j' \in \mathcal{N}(i) \setminus \{j\}} \Gamma_{j'}.$$

- (GD Step) If no Γ_j is updated in the previous sub-step: Find a $j \in \mathfrak{r}_2$ such that the corresponding column in \mathbf{H} has a maximum column weight. Set $\Gamma_j = -1$.
- Remove indices j from \mathfrak{r}_2 for which Γ_j was updated in this iteration.

Judgement. Do the same as in Algorithm 1, except that “Repeat from the Horizontal Step” is replaced by “Repeat from the step of Iterative Update”.

These symmetries in degenerate errors are observed in many QLDPC codes. We present the following proposition, which is supported by simulations in Sec. V.

Proposition 10. When columns in \mathbf{H} have minimal overlap, a bit-flipping decoder is likely to converge. In contrast, a stabilizer QLDPC code contains small stopping sets, leading to overlapping columns in \mathbf{H} . However, these overlapping columns usually exhibit strong symmetry (e.g., see [18, Fig. 4], [44]), and the GD step in Algorithm 1 is likely to find a feasible solution in Theorem 4 to support successful decoding.

Algorithm 1 can be run with full parallelism. If this is not required, the algorithm can be simplified as shown as in Algorithm 2. Algorithms 1 and 2 have the same performance in that if they encounter a stopping set, the GD step will be performed. However, Algorithm 2 may converge faster with fewer iterations. This comes at the cost of losing full parallelism, as the update of a Γ_j depends on another $\Gamma_{j'}$ that is subject to change within the same iteration. For convenience, we will simulate Algorithm 2 when evaluating the performance of GD Flip-BP₂.

Also note that Algorithm 2 is similar to a peeling decoder that the condition $|\mathcal{N}(i) \cap \mathbb{r}_2| = 1$ is called dangling check in the peeling decoder [34]. The raw peeling decoder also suffers from stopping sets, and a pruned peeling decoder improves this by flipping bits based on stabilizers (based on combinations of the rows of H). Furthermore, a VH technique is introduced to the pruned peeling decoder to improve the performance, focused on HP codes [34].

B. Soft-value based Quaternary BP

In GD Flip-BP₂, a hard change is made for Γ_j when it is determined to be +1 or -1 and this value does not change thereafter. It is possible that this decision is incorrect. Generally, we consider a soft-valued version of the decoder, where the messages are represented as soft values, allowing them to adjust their signs and magnitudes during iterations to facilitate increasingly precise decisions.

If a qubit j is erased, its initial error distribution is $(p_j^I, p_j^X, p_j^Y, p_j^Z) = (\frac{1}{4}, \frac{1}{4}, \frac{1}{4}, \frac{1}{4})$. Otherwise, the qubit is untouched and its initial error distribution is $(p_j^I, p_j^X, p_j^Y, p_j^Z) = (1, 0, 0, 0)$. We update the quaternary error distributions and treat them as soft vectors during iterations. The decoding becomes a quaternary BP (BP₄).

The update rules of BP₄, with respect to the symplectic inner product, are derived using probability theory in [48, 67]. In particular, a linear-domain BP₄ is given in [48], and an equivalent log-domain BP₄ is given [67]. Furthermore, a technique called *fixed inhibition*, which is shown to improve the perception capability of a decoding network [68–70], is introduced to BP₄ to become a quaternary BP with additional memory effects, called MBP₄ [45]. This decoder can be run with multiple instances in an adaptive way to become AMBP₄ to further improve the performance. For the detailed steps of (A)MBP₄, see [45].

The decoder (A)MBP₄ successfully decodes highly-degenerate codes compared to raw BP decoders, which need post-processing like ordered statistics decoding (OSD) [71] to resolve trapped quantum errors in raw BP [72, 73]. The OSD complexity is $O(n^3)$ due to the use of Gaussian elimination.

MBP₄ has scalar check-to-variable messages $\Delta_{i \rightarrow j}$ like Algorithm 1 but with soft values. A real parameter $\alpha > 0$ controls the BP update step-size by scaling each $\Delta_{i \rightarrow j}$ as $(1/\alpha)\Delta_{i \rightarrow j}$ before it is used to infer Γ_j . This is called message normalization [74, 75], and is usually used with $\alpha > 1$ in classical decoding to suppress wrong information looped

Algorithm 3 : Erasure decoding using (A)MBP₄

Input:

A check matrix $H \in \{I, X, Y, Z\}^{m \times n}$, a syndrome $\mathbf{s} \in \{0, 1\}^m$, erased coordinates $\mathbb{r} \subseteq \{1, 2, \dots, n\}$, an integer $T_{\max} > 0$, and a set of real $\alpha_1 > \alpha_2 > \dots > \alpha_\ell > 0$.

Initialization.

- Set $(p_j^I, p_j^X, p_j^Y, p_j^Z) = (\frac{1}{4}, \frac{1}{4}, \frac{1}{4}, \frac{1}{4})$ for $j \in \mathbb{r}$ and $(p_j^I, p_j^X, p_j^Y, p_j^Z) = (1, 0, 0, 0)$ for $j \in \mathbb{r}^c$.

Enclosed Decoder.

- Run (A)MBP₄($H, \mathbf{s}, T_{\max}, \{p_j^I, p_j^X, p_j^Y, p_j^Z\}_{j=1}^n, \{\alpha_i\}_{i=1}^\ell$) and obtain the estimate $\hat{E} \in \{I, X, Y, Z\}^n$ of BP.

Output.

- Return $\hat{E} \in \{0, 1\}^{2n}$ and an indicator of whether $\langle \hat{E}, H \rangle = \mathbf{s}$ or not, where \hat{E} and H are the binary version of \hat{E} and H , respectively.

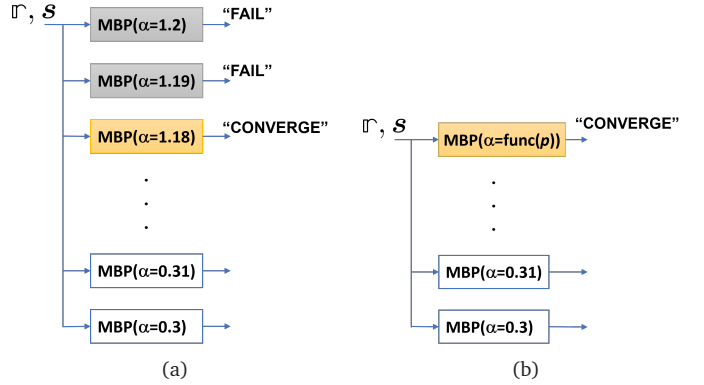


FIG. 4: (a) AMBP₄ with $\alpha_1, \alpha_2, \dots, \alpha_\ell$ set to 1.2, 1.19, \dots , 0.3. (b) The same as (a) but α_1 is a function of the physical error rate. Each MBP₄ instance is efficient, but on “FAIL,” it consumes T_{\max} iterations and needs time. In (a), two failed MBP₄ instances initially run with T_{\max} iterations. In (b), AMBP₄ achieves the efficiency of a successful MBP₄ by choosing an appropriate α_1 value (e.g., 1.18, when $\text{func}(p) = 1.18$, see Proposition 12).

in the cycles of the Tanner graph. This technique works well in the quantum case [48, 67]. However, for highly-degenerate codes, we may need $\alpha < 1$ to search for degenerate solutions with weights larger than the code’s classical distance [45].

MBP₄ is like a soft version of GD Flip-BP₂ and considers the quaternary error distribution.

AMBP₄ (sequentially) tests a list of $\alpha_1 > \alpha_2 > \dots > \alpha_\ell$ and chooses a best α^* from them adaptively [45]. We illustrate the procedure in Fig. 4(a). The value of α_1 can be selected as a function of the physical error rate, as shown in Fig. 4(b), to facilitate the efficiency, as we discuss later.

Both MBP₄ and AMBP₄ use the Pauli check matrix $H \in \{I, X, Y, Z\}^{m \times n}$, rather than a binary H , for quaternary decoding. To define the algorithms and their inputs with ini-

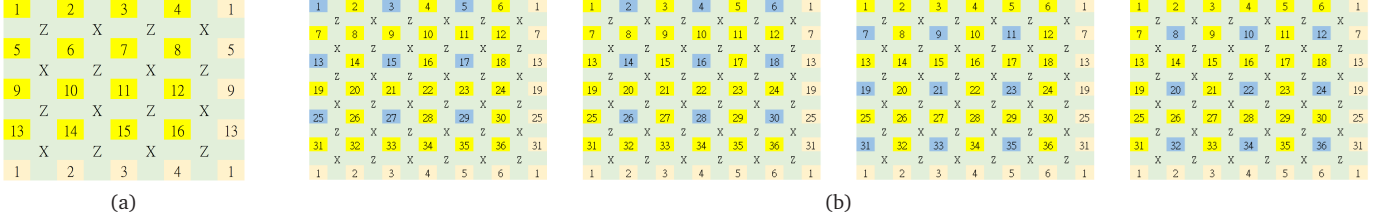


FIG. 5: (a) The lattice representation of the $[[16, 2, 4]]$ toric code. (b) The group random schedule run on the $[[36, 2, 6]]$ toric code.

In (a), a qubit is represented by a yellow box numbered from 1 to $n = 16$. Each orange box on the right and bottom represents the qubit of the same number. An X - or Z -type stabilizer is indicated by a label $W \in \{X, Z\}$ between its neighbouring qubits.

In (b), the figure shows that how a toric code is partitioned into 4 groups. Blue colour indicates which variable nodes are in one group.

tial error distributions in the linear domain, we write:

$$\text{MBP}_4(H, \mathbf{s}, T_{\max}, \{p_j^I, p_j^X, p_j^Y, p_j^Z\}_{j=1}^n, \alpha) \quad \text{and} \\ \text{AMBP}_4(H, \mathbf{s}, T_{\max}, \{p_j^I, p_j^X, p_j^Y, p_j^Z\}_{j=1}^n, \{\alpha_i\}_{i=1}^\ell).$$

Both output a convergence indicator and an estimate $\hat{E} \in I, X, Y, Z^n$. For a unified notation, we let $\ell = 1$ for MBP_4 and $\ell > 1$ for AMBP_4 and write:

$$(A)\text{MBP}_4(H, \mathbf{s}, T_{\max}, \{p_j^I, p_j^X, p_j^Y, p_j^Z\}_{j=1}^n, \{\alpha_i\}_{i=1}^\ell).$$

The decoder $(A)\text{MBP}_4$ is itself a GD using the information from all soft messages and all check values (see [45, arXiv]), and should outperform GD Flip-BP₂. An erasure decoding of using $(A)\text{MBP}_4$ is given in Algorithm 3. An important part is setting the initial distributions, as shown as in Algorithm 3. Another important part is letting the enclosed $(A)\text{MBP}_4$ perform a suitable soft approximation, which we discuss as follows.

Remark 11. When $(A)\text{MBP}_4$ is used, the message should be constrained to have suitable magnitude for numerical stability, to prevent overflow or underflow. This constraint also improves the erasure decoding, as the initial distributions $(1, 0, 0, 0)$ or $(\frac{1}{4}, \frac{1}{4}, \frac{1}{4}, \frac{1}{4})$ restrict the message to certain values out of the suitable range. With the constraint of message magnitude, a soft decoding is performed, improving the decoding performance. More specifically, the constraint makes the unknown variables to be computed as if there were a slight perturbation to the discrete messages in Algorithm 1. In Appendix A, we suggest how to implement the disturbance.

It is essential to select an appropriate value for the parameter α for $(A)\text{MBP}_4$. Recall that α acts as a scaling factor $\frac{1}{\alpha}$, functioning like a step-size adjustment for the BP updates. Intuitively, as the physical error rate p rises, the error weight increases, necessitating a smaller α to keep updates effective. We propose the following:

Proposition 12. The value of α decreases linearly with $\log(p)$ over a suitable range, and is approximately a linear function of p in a narrower range, denoted $\alpha = \text{func}(p)$.

This proposition can be proved from observing that the channel operation (6) resembles a depolarizing model (11).

Then it follows from a derivation for soft-valued GD updates in this model [45, arXiv]. We omit the derivation but refer to [45, arXiv Fig. 3] for the derived relation between α and the physical error rate: α approximates a function with a shape similar to $-\tanh(\log(p))$, which is approximately linear in p in a narrow range. Simulation results also validate Proposition 12 (see Sec. V A).

A remark for output is: In Algorithm 3, we could enforce $(\hat{E}_j^X | \hat{E}_j^Z) = (0|0)$ for $j \in \bar{r}$, before testing the syndrome and output. However, this is unnecessary because the initial distribution $(p_j^I, p_j^X, p_j^Y, p_j^Z) = (1, 0, 0, 0)$ for $j \in \bar{r}$ inherently enforces that $\hat{E}_j = I$ for $j \in \bar{r}$ in the BP output.

C. BP schedule and parallelism

When $(A)\text{MBP}_4$ is used, we consider two different schedules. The first is the parallel schedule, similar to Algorithm 1, and is as outlined in the original algorithm in [45].

The serial schedule offers the advantage of better convergence, especially when decoding QLDPC codes [45, 48]. We observe that randomizing the serial order in each iteration helps prevent the decoder from getting trapped in the same stopping set. To maintain parallelism, we propose a *group random schedule*, described as follows.

First, partition the variable nodes into groups based on a **partition rule**: Variable nodes that have independent messages within an iteration are assigned to the same group. Groups are processed in serial, and Variable nodes within a group are processed in parallel.

This is better illustrated by using topological codes. We show the 4×4 toric code in Fig. 5(a), explaining the code structure. Then we show the 6×6 toric code in Fig. 5(b), illustrating the partition of groups. The 36 variable nodes are partitioned into 4 groups using the above partition rule.

Next, we also use the toric codes to explain the group random schedule. For a toric lattice of size n , the group size is $n/4$ and there are four groups. If we have $n/4$ cores, the messages of all nodes within each group are processed in parallel. However, the four groups are processed in serial, and this serial order is randomized in each iteration. In software simulations, this is modelled by a random serial order, where one group is followed by another. The inter-

nal order of the nodes within a group does not affect the simulation of this schedule.

The group random schedule offers the advantage of high parallelism while maintaining strong convergence, and it is applicable to general QLDPC codes.

V. SIMULATIONS

We conduct computer simulations for HP and GHP codes [19], [72], bicycle codes [18], LP codes [21], and topological toric and XZZX codes [12–14], [15–17]. In all simulations, we set $T_{\max} = 100$. The average number of iterations is as low as $O(\log \log n)$ and the decoders exhibit as an MLD in many cases, as will be discussed later.

A. HP and GHP codes

Here, we use two medium-length codes to compare decoder performance and demonstrate the selection of (A)MBP parameters.

First, we consider the HP codes [19]. A $[[625, 25, 8]]$ HP code is examined in [73], [34] for depolarizing and erasure errors, respectively. We compare our decoders with three decoders from [34]: pruned peeling, pruned peeling + VH, and the Gaussian decoder. Since only half of the block of the (CSS) code is considered in [34], if they report a decoding failure rate f , we map it to $1 - (1 - f)^2$ as the logical error rate under consideration here.

The comparison is illustrated in Fig. 6. For (A)MBP decoders, MBP_4 employs $\alpha = 1$, and AMBP_4 selects α^* from $1.2, 1.19, \dots, 0.3$. The observations are as follow.

First, GD Flip- BP_2 performs comparably to the pruned peeling decoder, despite employing a simple GD approach. In contrast, the pruned peeling decoder searches through $\binom{m}{2}$ stabilizers to flip bits when escaping from a stopping set, where m is the number of rows in the check matrix. Second, MBP_4 demonstrates an improvement over GD Flip- BP_2 due to the use of soft messages. Third, AMBP_4 with parallel schedule is comparable to the pruned peeling + VH decoder. Finally, AMBP_4 with group random schedule achieves the best performance in Fig. 6.

In contrast, the Gaussian decoder in [34] does not attain optimal performance in Fig. 6. One possible explanation is that the authors treat the Gaussian decoder as a classical decoding strategy and mention that: it succeeds if $\hat{e} = e$. This approach, however, does not account for degeneracy.

We assess the performance of AMBP_4 by using Corollary 6. Table I presents the logical error rate and false convergence rate for AMBP_4 at different erasure error rates. The results demonstrate that AMBP_4 with group random schedule exhibits strong convergence, with the two error rates being very close. Consequently, this decoder closely approximates the behaviour of MLD for this code.

We observe that, at $p = 0.093$, the group random AMBP_4 requires an average of only 1.68 iterations. GD Flip- BP_2 is also efficient, requiring about 1.6 iterations on average at

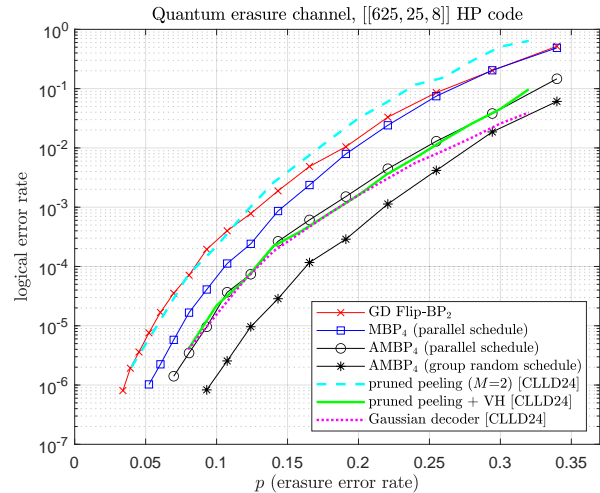


FIG. 6: Comparison of decoders on the $[[625, 25, 8]]$ HP code. The first four decoders are from this paper, and three others from [34] are labelled [CLLD24]. The Gaussian decoder in [CLLD24] does not achieve optimal performance, possibly due to a classical criterion (it succeeds if $\hat{e} = e$) mentioned. Group random AMBP_4 closely approaches MLD performance (see Table I).

TABLE I: Statistics of AMBP_4 for decoding the $[[625, 25, 8]]$ HP code at different erasure error rates p . Parallel AMBP_4 can be trapped by certain stopping sets, preventing convergence. In contrast, group random AMBP_4 resolves almost all encountered stopping sets, yielding closely matched false convergence and logical error rates, resembling an MLD (Corollary 6).

AMBP_4 (parallel)	$p=0.093$	$p=0.191$	$p=0.294$
false convergence rate	1.06×10^{-6}	0.000272	0.01065
logical error rate	9.61×10^{-6}	0.001509	0.03804

AMBP_4 (grp. rand.)	$p=0.093$	$p=0.191$	$p=0.294$
false convergence rate	7.79×10^{-7}	0.000252	0.01116
logical error rate	8.29×10^{-7}	0.000289	0.01861

$p = 0.093$, though its decoding accuracy is lower. We observe a similar low average number of iterations, approximately $O(\log \log n)$, for other codes as well.

Next, we focus on the group random schedule and compare (A)MBP₄ on a GHP code. Specifically, we demonstrate how to select an optimal value of α for MBP_4 , or an appropriate initial value α_1 for AMBP_4 .

Consider the $[[882, 48, 16]]$ GHP code from [72]. MBP_4 performance with different α values is shown in Fig. 7. As shown, there are three transition points at approximately $p = 0.32, 0.33$, and 0.34 , which correspond to optimal choices of $\alpha = 1.2, 1.0$, and 0.8 , respectively. This linear trend aligns with Proposition 12, establishing a linear relationship: $\alpha = -20p + 7.6p$.

For AMBP_4 , we propose the following choice for α_1 :

$$\alpha_1 = \text{func}(p) := \max(\min(-20p + 7.6, 1.2), 0.3), \quad (31)$$

where 1.2 serves as the upper bound for α_1 , and 0.3 is the

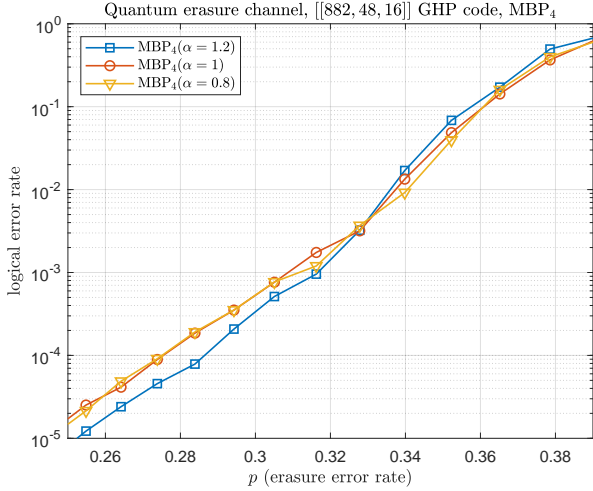


FIG. 7: MBP_4 performance on the $[[882, 48, 16]]$ GHP code using different values of α . There are three transition points at approximately $p = 0.32, 0.33$, and 0.34 , corresponding to optimal choices of $\alpha = 1.2, 1.0$, and 0.8 , respectively, establishing a linear relationship as suggested in Proposition 12.

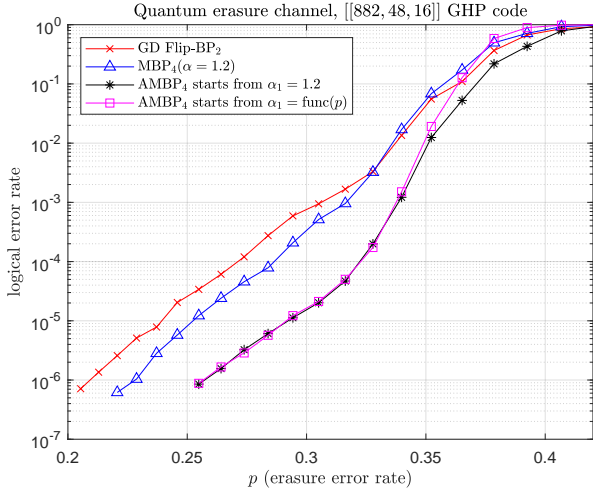


FIG. 8: Performance of several decoders on the $[[882, 48, 16]]$ GHP code. For $\alpha_1 = \text{func}(p)$ as defined in (31), AMBP_4 achieves performance similar to that with a fixed α_1 but with faster runtime, especially at high physical error rate (see Table II).

TABLE II: Average number of iterations for AMBP_4 on the $[[882, 48, 16]]$ GHP code. Both α_1 methods perform efficiently at low physical error rates, AMBP_4 with $\alpha_1 = \text{func}(p)$ provides significantly faster runtime at high physical error rate.

GD Flip₂ iterations are also shown for reference.

AMBP_4 avg. iter. \ p:	$p=0.255$	$p=0.328$	$p=0.392$
starts from $\alpha_1 = 1.2$	3.28	10.54	4628.89
starts from $\alpha_1 = \text{func}(p)$	3.28	8.33	90.27
GD Flip ₂ avg. iter.	2.99	5.18	51.51

value of the last α_ℓ that we intend to set. A broader range of values does not yield further performance improvements.

We evaluate two AMBP_4 strategies: the first with

$$\alpha^* \in \{1.2, 1.19, \dots, 0.3\},$$

and the second with

$$\alpha^* \in \{\text{func}(p), \text{func}(p) - 0.01, \dots, 0.3\}.$$

We present (A) MBP_4 performance in Fig. 8. As shown, the two strategies exhibit similar performance. Upon reviewing the raw data, we note that when $p \leq 0.328$ (when AMBP_4 logical error rate $< 10^{-4}$), AMBP_4 displays approximately equal logical error and false convergence rates, indicating that it exhibits like an MLD (Corollary 6). Both strategies also show similar average numbers of iterations when $p \leq 0.328$, as detailed in Table II. However, a significant difference arises at higher physical error rate, such as $p = 0.392$. In this case, AMBP_4 with a fixed α_1 requires many more iterations. This is because α^* is smaller at higher values of p , leading the decoder to potentially run up to T_{\max} iterations for each larger α_i that fails to converge.

As noted above, using a fixed α_1 is effective over a wide range of p . In the following, we will use a fixed α_1 and select an appropriate value if AMBP_4 is employed.

B. Bicycle codes

Bicycle codes offer flexible length and rate, and demonstrate performance close to the quantum Gilbert-Varshamov bound for correcting depolarizing errors [18, 45].

We construct bicycle codes with varying code rates $r = \frac{k}{n}$ and row-weights w using random generator vectors. A key step in this construction is row-deletion, which requires heuristic methods [18, 67]². The bicycle construction results in a Pauli check matrix with a mean column-weight $j \approx w(1-r)$. We construct three families of bicycle codes:

- Rate 1/4, $w = 12$: $n = 946, 1892, 3786$. (Mean column-weight $j \approx 9$.)
- Rate 1/2, $w = 18$: $n = 946, 1892, 3786$. (Mean column-weight $j \approx 9$.)
- Rate 3/4, $w \approx 36$: $n = 946, 1892, 3786$ with $w = 34, 36, 38$, respectively. (Mean column-weight $j \approx 9$.)

First, we present the performance of GD Flip-BP₂, as shown in Fig. 9, and compare it with that of eBDD (12). The decoder performance aligns closely with eBDD for specific t/n ratios at each code rate, up to a point where an error-floor emerges, if present. The value t/n captures an

² Herein, we employ a greedy algorithm that deletes a group of 32 rows at a time, until there remains 64 rows to be deleted, one at a time, while maintaining small column-weight variance throughout the process.

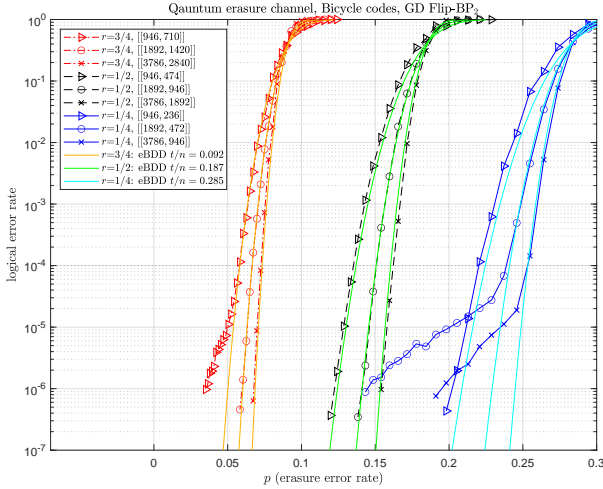


FIG. 9: GD Flip-BP₂ performance on bicycle codes. The decoder performs well, with error-floors primarily attributed to the codes, except in the case of [[1892, 472]] bicycle code (see Table III).

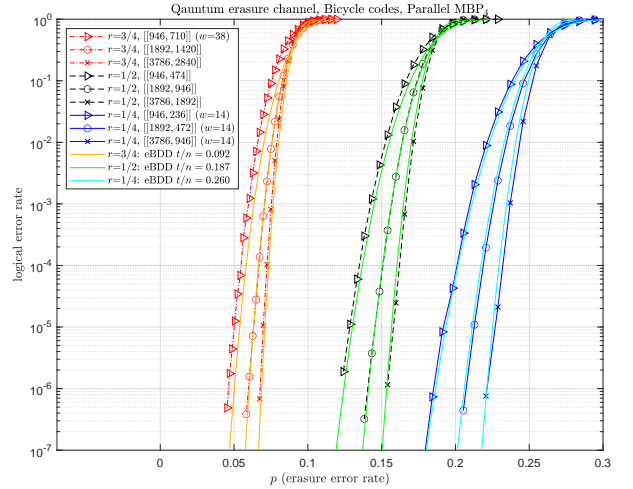


FIG. 11: Revisiting Fig. 10 with higher row-weight w for selected codes. Cases with increased w , indicated in the legend, show no error floor in comparison to Fig. 10. (Rate 3/4 codes achieve a threshold near $p \approx 1$ without error floors, highlighting an important application discussed in Sec. VI.)

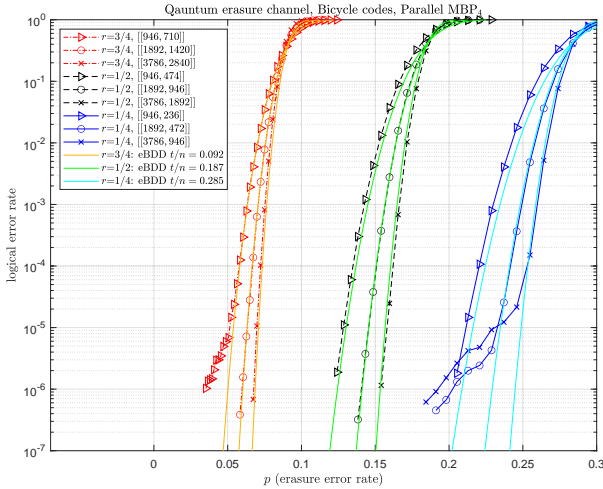


FIG. 10: Parallel MBP₄ performance on bicycle codes. The decoder performs closely to MLD for logical error rate below 10^{-4} , notably improving the [[1892, 472]] code over Fig. 9. The remaining error floor is mainly due to the code (see Table III).

TABLE III: Statistics of GD Flip-BP₂ and MBP₄ for decoding the [[1892, 472]] bicycle code with row-weight $w = 12$. MBP₄ improves upon GD Flip-BP₂ with a tenfold reduction in logical error rate, which closely matches the false convergence rate. Hence, MBP₄ nearly resembles MLD performance (Corollary 6).

GD Flip-BP ₂	$p=0.198$	$p=0.213$	$p=0.229$
false convergence rate	7.36×10^{-7}	2.24×10^{-6}	3.57×10^{-6}
logical error rate	9.2×10^{-6}	1.49×10^{-5}	2.75×10^{-5}
MBP ₄ (parallel)	$p=0.198$	$p=0.213$	$p=0.229$
false convergence rate	3.77×10^{-7}	1.28×10^{-6}	3.12×10^{-6}
logical error rate	6.7×10^{-7}	2×10^{-6}	4.27×10^{-6}

estimated threshold value at each code rate (Proposition 1). GD Flip-BP₂ is well-suited for decoding bicycle codes when extremely low decoding complexity is required.

Next, we present the performance of parallel MBP₄ (with $\alpha = 1$), as illustrated in Fig. 10. In comparison to Fig. 9, MBP₄ outperforms GD Flip-BP₂, resulting in lower error-floors. Specifically, MBP₄ typically demonstrates similar levels of logical error and false convergence rates for logical error rates below 10^{-4} . In Table III, we show the two error rates for both decoders on the [[1892, 472]] bicycle code, where the decoders exhibit the greatest performance difference. MBP₄ has these two error rates close to each other, performing similarly to an MLD (Corollary 6). This also suggests that the error-floor primarily arises from the code itself, rather than from the decoder.

In the classical setting, codes with logical error-floors below 10^{-2} are considered usable [25]. For quantum codes, we aim for a lower error-floor, below 10^{-4} [18, 45, 76]. The results in Figs. 9 and 10 meet this criterion.

Codes with the same rate exhibit consistent t/n eBDD performance. We estimate an error threshold for each code rate using this ratio t/n of eBDD (Proposition 1). The estimated thresholds are approximately 0.092, 0.187, and 0.285 for rates 3/4, 1/2, and 1/4, respectively.

In some cases, redoing the code construction may lower the error-floor. However, optimizing codes with low row-weight w is challenging because the row-deletion step can leave some columns with very low weights, resulting in insufficient protection for certain qubits.

An alternative strategy to address error-floors is to increase the row-weight w . The classical and quantum distances of a bicycle code are equal and upper bounded by the row-weight (i.e., $d' = d \leq w$) [18]. As a result of Remark 8,

the stopping number is bounded by w . By increasing w , we raise this bound, which improves the performance for codes experiencing error-floors. The improved results are shown in Fig. 11. However, as also shown, this comes at the cost of delayed waterfall of the curve, causing a reduced threshold 0.26 for codes with rate 1/4.

C. LP codes

Product codes generally perform well at low code rates. We focus on quantum LP codes [21] constructed from classical quasi-cyclic (QC) matrices [32, 77]. We observe that AMB_4 exhibits like an MLD for these codes (Corollary 6).

In this subsection, j, w, m and the girth value represent the parameters of the underlying QC matrix.

A QC matrix is defined by a $j \times w$ base matrix, where each entry represents a circulant matrix with a specific cyclic shift from an $m \times m$ identity matrix. This results in a sparse binary $jm \times wm$ QC matrix, which we use to construct an LP code with parameters $n = m(w^2 + j^2)$ and $k \geq m(w - j)^2$ [21]. The asymptotic rate is given by $r = (w - j)^2 / (w^2 + j^2)$.

The constructed QC matrix is regular. Regular QC matrices are known to produce classical codes with very low error-floors [46, 47]. Incorporating some $m \times m$ zero matrices in a QC matrix yields an irregular QC matrix, potentially increasing the girth of the classical code and causing the performance curve to exhibit a waterfall shape earlier [79], though a low error-floor is not guaranteed. We observe that these characteristics also apply in the quantum case.

We construct regular and irregular QC matrices following the techniques described in [80]. The constructed base matrices are detailed in Appendix B. Using these QC matrices, we then construct quantum LP codes, with parameters outlined in Table IV. Additionally, we consider two codes: an LP code from [21] (labelled [PK22]) and another LP code from [78] (labelled [Rav+22]), also outlined in Table IV.

We apply AMB_4 , selecting α^* from 1.2, 1.19, ..., 0.3, with the group random schedule for message updates. For $(j, w) = (3, 5)$, the asymptotic rate is approximately 0.118. The decoding performance is presented in Fig. 12. The code [Rav+22] exhibits an error-floor, while the code [PK22] not, despite their similar parameters. The key distinction lies in the QC matrices: [Rav+22] employs a typical QC matrix [77] containing many identity sub-matrices, whereas [PK22] utilizes a fully random QC matrix featuring random circulant shifts in each sub-matrix [32].

We construct longer codes, including two regular and one irregular code, all employing fully random QC matrices. For regular LP codes with rate 0.118, based on Fig. 12, we estimate a threshold of 0.368 (Proposition 1). Notably, this threshold is conservative, as the irregular code shows better performance at a logical error rate of 10^{-5} .

Next, we consider $(j, w) = (3, 4)$, which results in LP codes with an asymptotic rate of 0.04. The decoding performance is shown in Fig. 13. For this LP code rate, the threshold estimated from regular codes is 0.405. Notably, when $m \geq 37$, constructing random QC matrices with girth

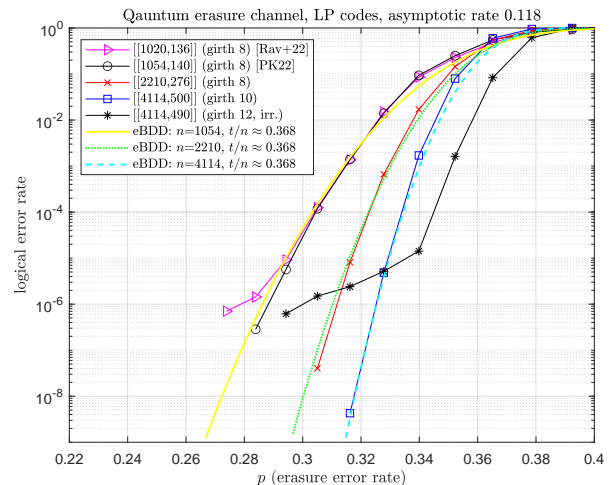


FIG. 12: Near-MLD performance of AMB_4 on rate 0.118 LP codes. Regular codes show a threshold $p_{\text{th}} = 0.368$. An irregular code performs better but is more prone to error floors. The regular codes [Rav+22] ([78]) and [PK22] ([21]) show [PK22] outperforms due to using a fully random base matrix from [32].

TABLE IV: Parameters of the LP codes employed in this paper.

Asymptotic rate 0.118:						
j	w	m	girth	$[[n, k]]$	irregular	from
3	5	30	8	$[[1020, 136]]$		[Rav+22]
3	5	31	8	$[[1054, 140]]$		[PK22] [†]
3	5	65	8	$[[2210, 276]]$		this paper
3	5	121	10	$[[4114, 500]]$		this paper
3	5	121	12	$[[4114, 490]]$	✓	this paper

[†] The base matrix is from [32].

Asymptotic rate 0.04:						
j	w	m	girth	$[[n, k]]$	irregular	from
3	4	37	8	$[[925, 49]]$		this paper
3	4	37	10	$[[925, 41]]$	✓	this paper
3	4	83	10	$[[2075, 95]]$		this paper
3	4	83	12	$[[2075, 95]]$		this paper
3	4	163	10	$[[4075, 175]]$		this paper

greater than 8 becomes easier. Since the stopping number increases exponentially for girth greater than 8 (Remark 7), the impact of varying girth values on performance tends to be insignificant. For $n = 2075$, we test girths of 10 and 12, which yield similar performance. Additionally, the estimated threshold is conservative; for $n = 925$, we construct an irregular code that shows improved performance, with no error-floor observed at a logical error rate of 10^{-6} .

If MLD performance is not essential, GD Flip-BP₂ demonstrates strong performance on LP codes. We compare it to AMB_4 in Fig. 14 at rate 0.118. As illustrated, GD Flip-BP₂ achieves performance close to AMB_4 , particularly as code length increases, although a logical error-floor may appear.

The threshold value can be estimated from the intersection of the performance curves. However, this method may overestimate the decoder performance, especially for de-

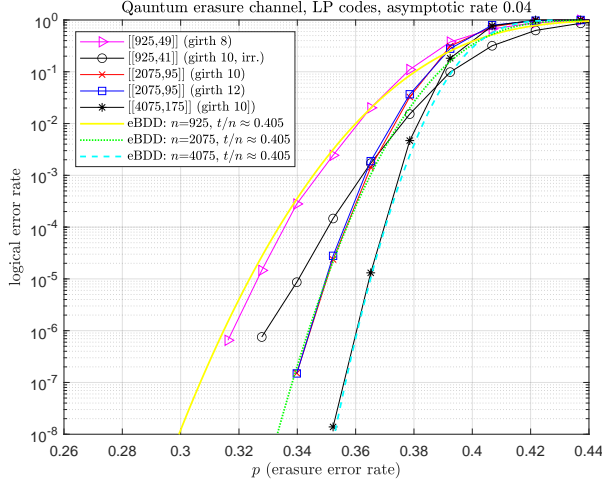


FIG. 13: Near-MLD performance of AMBP_4 on rate 0.04 LP codes. Regular codes show a threshold $p_{\text{th}} = 0.405$. An irregular code performs better at code length 925. Two regular codes of length 2075, both with girth > 8 , perform similarly (cf. Remark 7).

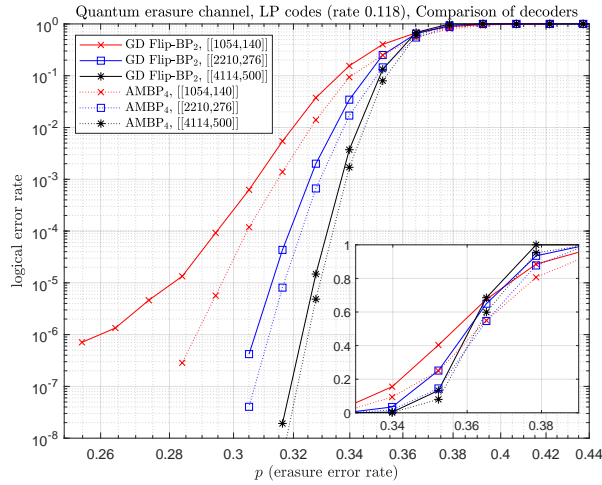


FIG. 14: GD Flip- BP_2 vs AMBP_4 on rate 0.118 LP codes. GD Flip- BP_2 performs closely to AMBP_4 , especially for larger codes. This figure also indicates that focusing solely on threshold performance may overlook possible error-floors.

coders not functioning as MLD. For instance, in Fig. 14, GD Flip- BP_2 exhibits a higher p value at the intersection but ultimately underperforms compared to AMBP_4 . In addition, focusing solely on threshold performance may overlook possible error-floors.

D. Topological codes

For topological codes, we consider (rotated) toric codes with parameters $[[L^2, 2, L]]$ for even L and (twisted) XZZX codes with parameters $[[\frac{(d^2+1)}{2}, 1, d]]$ for odd d (see [12, 14], [15], or a summary in [81, Table I]). We observe

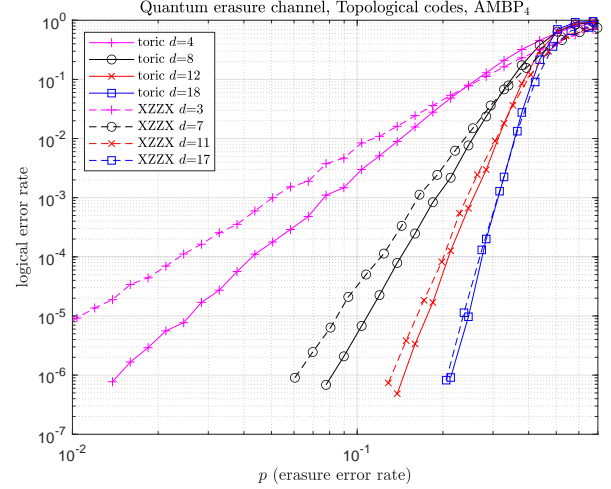


FIG. 15: Near-MLD performance of AMBP_4 on the toric and XZZX codes, each with a threshold at approximately $p = 0.5$ (Fig. 16).

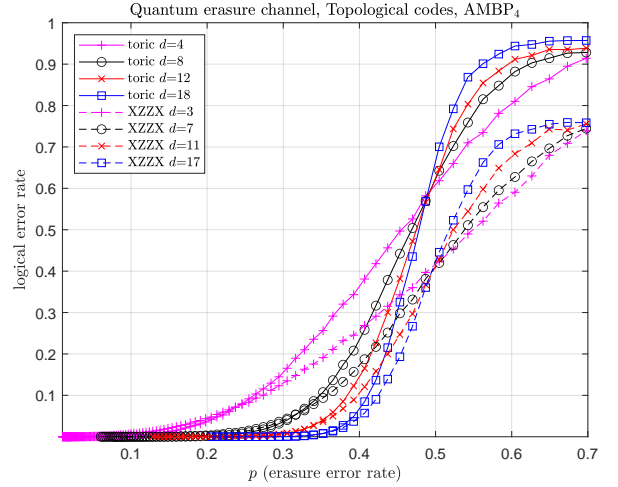


FIG. 16: Replotting Fig. 15 with p on a linear scale. AMBP_4 achieves thresholds close to 0.5 on the toric and XZZX codes. A topological code family has a threshold indicated by the intersection (Nishimori point) [13].

that AMBP_4 attains MLD for these codes (Corollary 6).

Although topological codes have vanishing rate $\frac{k}{n} \rightarrow 0$ as n increases, they can operate effectively at high erasure error rate p with a threshold approximately 0.5 [82, 83]. Therefore, we use a larger step size $1/\alpha$ to meet a higher value of p (Proposition 12). For AMBP_4 , we select $\alpha_1 = 0.95$ instead of 1.2. The performance of AMBP_4 with group random schedule is shown in Fig. 15. Both code families exhibit similar performance, with notable improvements as the code length increases.

For codes in a two-dimensional (or three-dimensional) model, the intersection of performance curves provides an estimate of the critical error probability, known as the Nishimori point, which represents the error threshold [13]. The

toric and XZZX codes are two-dimensional codes. We replot Fig. 15 with p on a linear scale in Fig. 16, showing that the estimated thresholds for both code families are close to 0.5.

We note that GD Flip-BP₂ performs similarly to AMBP₄ for $d \leq 12$ but encounters performance saturation for larger d . This can be improved by using AMBP₄ as a post-decoder, conveniently implemented by reusing Tanner graph structure. With this approach, when GD Flip-BP₂ achieves a low logical error rate (e.g., 10^{-2}), the overall computational complexity remains low on average.

E. Channel capacity and the thresholds of various codes

Using the results from the previous subsections, we analyse the performance of our decoders in comparison to the quantum erasure channel capacity [10]. The results are illustrated in Fig. 17. Using our decoders, we achieve near-capacity performance with topological codes for rate $r \rightarrow 0$. For $r > 0$, LP and bicycle codes yield performance approximately equal to $r = 1 - 2.5p$. For bicycle codes with a rate of 1/4, the threshold is estimated to be between 0.26 and 0.285, with the latter value confidently achievable if the error-floor issue is resolved.

We observe that physical fidelity decays exponentially over time (a behaviour characterized by the decoherence time) [3, 84]. To depict this physical effect, we replot Fig. 17 with p on a log scale in Fig. 18. From this figure, the tested codes exhibit performance approaching capacity.

In Fig. 18, we also plot rate upper bounds estimated in [59, Theorem 3.8], which depend on stabilizer weight w . Although these bounds are not necessarily tight, their trend is consistent with our findings in that higher code rates require higher w . For our tested codes: bicycle codes have stabilizer weights of roughly 36, 18, and 12, for rates 3/4, 1/2, and 1/4, respectively; regular LP codes have stabilizer weights of 8 and 7 for rates 0.118 and 0.04, respectively; and toric and XZZX codes have stabilizer weight of 4.

VI. DISCUSSIONS

We analysed the general quantum erasure decoding problem, and proposed efficient decoders suitable for this task. The GD flipping decoder performs exceptionally well on bicycle and LP codes, despite its extremely low complexity. The (A)MBP decoders exhibit behaviour similar to an MLD for various QLDPC codes tested, achieving near-capacity performance or a performance of $r = 1 - 2.5p$.

We apply our results on concatenated QLDPC codes with $[[\ell, 1]]$ permutation-invariant (PI) codes [49, 50, 85–88] as inner codes. Deletion errors can be catastrophic for stabilizer codes, but PI codes can correct them [50, 89]. Compared to the erasure error model, a primary challenge in the deletion error model is the lack of error location information, which makes decoding more difficult since misidentifying even one location can cause failure. While accurately locating every error location to obtain erasure errors

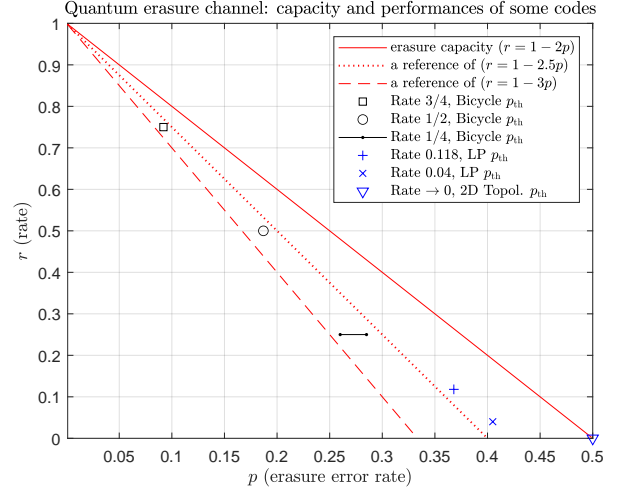


FIG. 17: Quantum erasure capacity and thresholds of codes. The capacity is $r = 1 - 2p$. Topological codes reach the capacity, with $r \rightarrow 0$. Other codes achieve approximately $r = 1 - 2.5p$ for $r > 0$.

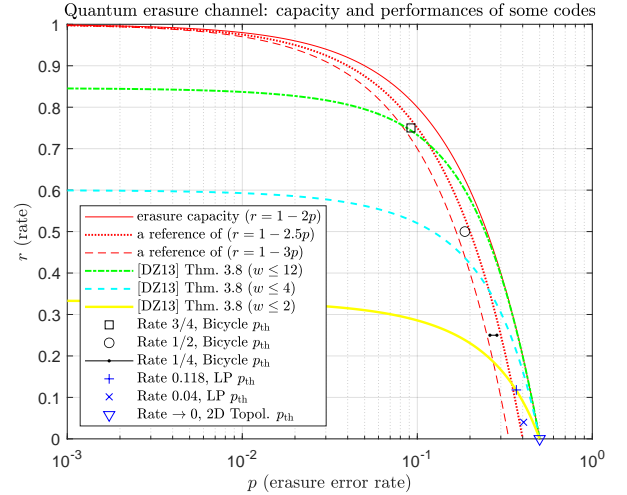


FIG. 18: Replotting Fig. 17 with p on a log scale. The tested codes exhibit performance approaching capacity, with higher-rate codes requiring larger stabilizer weight w . Furthermore we achieve $r = 3/4$ with $p \approx 0.1$. We compare our results with rate upper bounds from [59] ([DZ13]).

can assist decoding, it is time-consuming and increases error rates. Thus, accepting imperfect erasure conversions, where some leakage errors remain as localized deletions, can be more effective. Here, we assume a local deletion error model where the boundary of each block of ℓ physical qubits is identifiable. Each block is protected by an $[[\ell, 1]]$ PI code, which converts deletion errors to erasures after correction. We calculate the performance of this deletion to erasure conversion in Fig. 19, when each qubit within each inner code that corrects t deletions is deleted with probability ϵ . The $[[4, 1]]$ PI code [49, 90, 91] converts local deletions with probability up to 0.385 into erasure errors of rate less than 0.5, which topological codes can subsequently

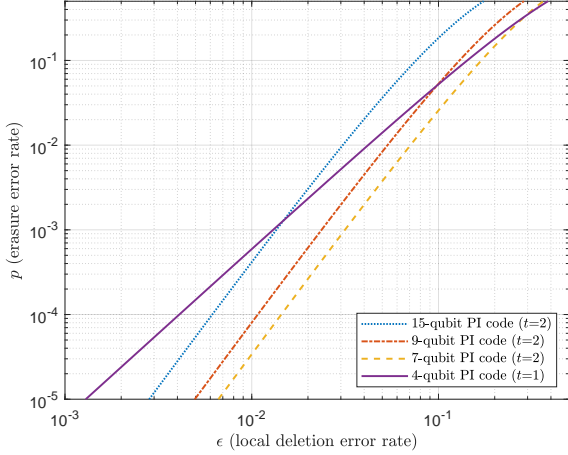


FIG. 19: Erasure error rate converted from local deletion error rate using $[[\ell, 1]]$ PI codes for $\ell = 4, 7, 9, 15$ ([49, 91], [86], [85], [92]). A $[[\ell < 15, 1]]$ PI code PI codes can convert high local deletion rates $\epsilon \approx 0.1$ to an erasure rate $p < 0.1$. The erasures are manageable by concatenating a QLDPC code with a high rate of $3/4$ (cf. Fig. 18).

decode. Longer PI codes reduce the erasure rate further for lower deletion probabilities, enabling reliable decoding when combined with higher-rate QLDPC codes. If the converted erasure error rate is less than 0.1, the QLDPC code rate exceeds $3/4$.

In a large system, after converting dominant noise into erasures at known locations, there may be additional or background error equilibria that lead to depolarizing errors on the received qubits. Using (A)MBP₄, we adapt by adjusting the initial error distribution for the non-erased qubits to $(p^I, p^X, p^Y, p^Z) = (1 - p_0, \frac{p_0}{3}, \frac{p_0}{3}, \frac{p_0}{3})$, where p_0 can be set to either the depolarizing error rate p_{dep} or a suitable fixed value [45, 67]. This adjustment enables the decoder to simultaneously correct for both erasure and depolarizing errors. In Fig. 20, we present results using the $[[1054, 140]]$ LP code, considering $p_{\text{dep}} = 0.01$. As shown, GD Flip-BP₂ always fails to decode because it cannot manage depolarizing errors and requires modifications. In contrast, (A)MBP₄ successfully handles both erasure and depolarizing errors, with AMBP₄ demonstrating impressive performance.

Our findings highlight the adaptability and effectiveness of the proposed decoders, illustrating their potential for handling diverse error types—erasure, deletion, and depolarizing errors—in complex quantum systems.

VII. ACKNOWLEDGEMENTS

K.K. and Y.O. acknowledge support from EPSRC (Grant No. EP/W028115/1).

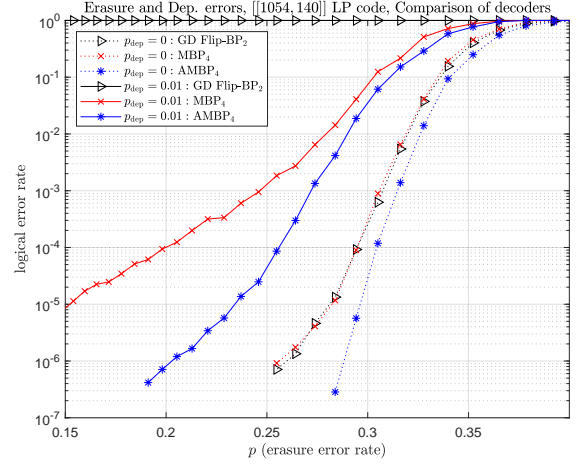


FIG. 20: Comparison of decoders handling erasure and depolarizing errors simultaneously. AMBP₄ maintains strong performance in this mixed error model.

Appendix A: Numerical stability and message softization

When a soft-valued BP algorithm, such as (A)MBP₄, is employed, message values must be constrained to ensure numerical stability. Based on our experience, the initial distributions do not require adjustment; the most effective approach is to constrain the variable-to-check messages.

The decoder (A)MBP₄ has each variable-to-check message representing a binary distribution $(q_{j \rightarrow i}^{(0)}, q_{j \rightarrow i}^{(1)})$, where $q_{j \rightarrow i}^{(0)} \in [0, 1]$ and $q_{j \rightarrow i}^{(1)} = 1 - q_{j \rightarrow i}^{(0)}$ (as in linear-domain MBP₄ [45, arXiv Alg. 3]³). To maintain numerical stability, we impose a stricter constraint: $q_{j \rightarrow i}^{(0)} \in (0, 0.5) \cup (0.5, 1)$. As shown in Box 1, this is achieved by introducing a small disturbance δ to $q_{j \rightarrow i}^{(0)}$ when $q_{j \rightarrow i}^{(0)}$ is too close to 0, 0.5, or 1. A recommended value of δ is 10^{-10} by MacKay [47]. For our purposes, we adopt 10^{-11} , which enhances accuracy while preserving numerical stability⁴.

The information $(q_{j \rightarrow i}^{(0)}, q_{j \rightarrow i}^{(1)})$ is conveyed by a scalar message $d_{j \rightarrow i} = q_{j \rightarrow i}^{(0)} - q_{j \rightarrow i}^{(1)} \in [-1, +1]$. This is like a soft generalization compared to Algorithm 1, which limits messages to three discrete values: $-1, 0, \text{ or } +1$. Messages with values ± 1 can lead to numerical instability, while 0-valued messages trap the decoder in stopping sets. Introducing the disturbance δ constrains $d_{j \rightarrow i}$ to the range $(-1, 0) \cup (0, +1)$, thereby mitigating these issues and enabling soft message updates for computing the required probabilities.

³ The quantity $q_{j \rightarrow i}^{(0)}$ is the probability that Pauli error E_j at qubit j commutes with check-matrix entry H_{ij} .

⁴ This calculation in Box 1 considers a quaternary check matrix with row-weight 30 and assumes a worst-case scenario where all incoming messages to a check node are at extreme values, a situation that is rare. Even if row-weight > 30 and underflow (or overflow) occurs, subsequent iterations restore stability by reapplying the constraint on $(q_{j \rightarrow i}^{(0)}, q_{j \rightarrow i}^{(1)})$.

```

/-- prevent extreme linear values
#define dlt (1e-11) // note, log10((2e-11)^30) = -320.97 (still > DBL_MIN 5e-324 even if row_wt=30);
#define restrict_p2(p) \
{ \
  if(p[0] < dlt_b) { \
    p[0] = dlt_b;    p[1] = 1.0 - dlt_b; \
  } \
  else if(p[0] > 1.0 - dlt_b) { \
    p[0] = 1.0 - dlt_b;    p[1] = dlt_b; \
  } \
  else if(0.5-dlt_b < p[0] && p[0] < 0.5+dlt_b) { \
    if(p[0] < 0.5) { p[0] = 0.5-dlt_b; p[1] = 0.5+dlt_b; } \
    else { p[0] = 0.5+dlt_b; p[1] = 0.5-dlt_b; } \
  } \
  else { p[1] = 1.0 - p[0]; } \
}

```

Box 1

```

/-- prevent extreme LLR values
// #define LLR_MAX (38) // IEEE754 double 1.0-tanh(38.2/2) = 1.110223024625157e-16 , but 1.0-tanh(38.2/2) = 0 (NG)
// #define LLR_MAX (36) // very extreme since if >36, sometimes makes LLR decoder messages Dm[m]=0
#define LLR_MAX (35) // IEEE754 double tanh(35.9/2) = 0.9999999999999999 , protected from tanh(36/2) = 1 (OK)
#define prevent_llr_ov(llr) { \
  if(llr > LLR_MAX) { llr = LLR_MAX; } \
  else if(llr < -LLR_MAX) { llr = -LLR_MAX; } \
}
/-- prevent LLR to be too close to zero
#define LLR_MIN (1.0e-10) // support up to row weight 30, since tanh(1e-10/2)^30 = 9.313225746154796e-310 ~ = |DBL_MIN|
#define prevent_llr_0(llr) { \
  if(llr < LLR_MIN) { \
    if(llr >= 0) { llr = LLR_MIN; } \
    else if(llr > -LLR_MIN) { llr = -LLR_MIN; } \
  } \
}
/-- restrict LLR in reasonable range
#define restrict_llr(llr) { \
  if(llr > LLR_MAX) { llr = LLR_MAX; } \
  else if(llr < -LLR_MIN) { \
    if(llr >= 0) { llr = LLR_MIN; } \
    else if(llr > -LLR_MIN) { llr = -LLR_MIN; } \
    else if(llr < -LLR_MAX) { llr = -LLR_MAX; } \
  } \
}

```

Box 2

The (A)MBP₄ algorithm can also operate in the log domain, where the distribution $(q_{j \rightarrow i}^{(0)}, q_{j \rightarrow i}^{(1)})$ is expressed as a log-likelihood ratio (LLR), $\ln(q_{j \rightarrow i}^{(0)}/q_{j \rightarrow i}^{(1)})$ (which corresponds to the scalar message $\lambda_{S_{mn}}(\Gamma_{n \rightarrow m})$ in the LLR MBP₄ [45, arXiv Alg. 1]). Box 2 demonstrates how constraints are applied to log-domain messages.

Appendix B: Base matrices for the constructed LP codes

We provide the base matrices for the QC matrices used in the LP codes constructed in this paper (Table IV). In these base matrices, a value of 0 indicates an $m \times m$ identity sub-matrix, while -1 signifies an $m \times m$ zero sub-matrix.

For asymptotic rate 0.118:

$$m = 65; \quad \text{girth } 8; \quad \begin{bmatrix} 30 & 32 & 57 & 37 & 23 \\ 19 & 7 & 53 & 64 & 47 \\ 47 & 7 & 63 & 37 & 21 \end{bmatrix}. \quad (\text{B1})$$

$$m = 121; \quad \text{girth } 10; \quad \begin{bmatrix} 55 & 60 & 106 & 118 & 88 \\ 36 & 13 & 95 & 70 & 37 \\ 86 & 13 & 71 & 44 & 31 \end{bmatrix}. \quad (\text{B2})$$

$$m = 121; \quad \text{girth } 12; \quad \begin{bmatrix} 4 & 92 & 117 & 81 & 76 \\ 93 & 51 & 108 & 85 & -1 \\ 107 & 77 & 84 & 6 & 12 \end{bmatrix} \text{ (irregular)}. \quad (\text{B3})$$

For asymptotic rate 0.04:

$$m = 37; \quad \text{girth } 8; \quad \begin{bmatrix} 17 & 19 & 33 & 21 \\ 11 & 4 & 31 & 0 \\ 27 & 4 & 36 & 21 \end{bmatrix}. \quad (\text{B4})$$

$$m = 37; \quad \text{girth } 10; \quad \begin{bmatrix} 17 & 19 & 33 & 21 \\ 11 & 4 & 29 & 18 \\ 27 & 5 & 35 & -1 \end{bmatrix} \text{ (irregular)}. \quad (\text{B5})$$

$$m = 83; \quad \text{girth } 10; \quad \begin{bmatrix} 38 & 41 & 73 & 47 \\ 25 & 9 & 65 & 42 \\ 59 & 9 & 81 & 62 \end{bmatrix}. \quad (\text{B6})$$

$$m = 83; \quad \text{girth } 12; \quad \begin{bmatrix} 58 & 77 & 30 & 3 \\ 23 & 0 & 64 & 47 \\ 58 & 23 & 82 & 35 \end{bmatrix}. \quad (\text{B7})$$

$$m = 163; \quad \text{girth } 10; \quad \begin{bmatrix} 74 & 80 & 143 & 92 \\ 48 & 18 & 129 & 159 \\ 116 & 17 & 156 & 84 \end{bmatrix}. \quad (\text{B8})$$

- [1] D. Bluvstein, S. J. Evered, A. A. Geim, S. H. Li, H. Zhou, T. Manovitz, S. Ebadi, M. Cain, M. Kalinowski, D. Hangleiter, *et al.*, Logical quantum processor based on reconfigurable atom arrays, *Nature* **626**, 58 (2024).
- [2] P. Scholl, A. L. Shaw, R. B.-S. Tsai, R. Finkelstein, J. Choi, and M. Endres, Erasure conversion in a high-fidelity Rydberg quantum simulator, *Nature* **622**, 273 (2023).
- [3] S. Ma, G. Liu, P. Peng, B. Zhang, S. Jandura, J. Claes, A. P. Burgers, G. Pupillo, S. Puri, and J. D. Thompson, High-fidelity gates and mid-circuit erasure conversion in an atomic qubit, *Nature* **622**, 279 (2023).
- [4] Y. Wu, S. Kolkowitz, S. Puri, and J. D. Thompson, Erasure conversion for fault-tolerant quantum computing in alkaline earth Rydberg atom arrays, *Nat. Commun.* **13**, 4657 (2022).
- [5] I. Cong, H. Levine, A. Keesling, D. Bluvstein, S.-T. Wang, and M. D. Lukin, Hardware-efficient, fault-tolerant quantum computation with Rydberg atoms, *Phys. Rev. X* **12**, 021049 (2022).
- [6] A. Kubica, A. Haim, Y. Vaknin, H. Levine, F. Brandão, and A. Retzker, Erasure qubits: Overcoming the T_1 limit in superconducting circuits, *Phys. Rev. X* **13**, 041022 (2023).
- [7] J. D. Teoh, P. Winkel, H. K. Babla, B. J. Chapman, J. Claes, S. J. de Graaf, J. W. Garmon, W. D. Kalfus, Y. Lu, A. Maiti, *et al.*, Dual-rail encoding with superconducting cavities, *Proc. Nat. Acad. Sci. (PNAS)* **120**, e2221736120 (2023).
- [8] H. Levine, A. Haim, J. S. Hung, N. Alidoust, M. Kalae, L. DeLorenzo, E. A. Wollack, P. Arrangoiz-Arriola, A. Khalajhedayati, R. Sanil, *et al.*, Demonstrating a long-coherence dual-rail erasure qubit using tunable transmons, *Phys. Rev. X* **14**, 011051 (2024).
- [9] C.-Y. Lu, W.-B. Gao, J. Zhang, X.-Q. Zhou, T. Yang, and J.-W. Pan, Experimental quantum coding against qubit loss error, *Proc. Natl. Acad. Sci. (PNAS)* **105**, 11050 (2008).
- [10] C. H. Bennett, D. P. DiVincenzo, and J. A. Smolin, Capacities of quantum erasure channels, *Phys. Rev. Lett.* **78**, 3217 (1997).
- [11] S. B. Bravyi and A. Y. Kitaev, Quantum codes on a lattice with boundary, arXiv preprint quant-ph/9811052 10.48550/arXiv.quant-ph/9811052 (1998).
- [12] A. Y. Kitaev, Fault-tolerant quantum computation by anyons, *Ann. Phys.* **303**, 2 (2003), preprint arXiv: quant-ph/9707021 (1997).
- [13] E. Dennis, A. Kitaev, A. Landahl, and J. Preskill, Topological quantum memory, *J. Math. Phys.* **43**, 4452 (2002).
- [14] H. Bombin and M. A. Martin-Delgado, Optimal resources for topological two-dimensional stabilizer codes: Comparative study, *Phys. Rev. A* **76**, 012305 (2007).
- [15] A. A. Kovalev, I. Dumer, and L. P. Pryadko, Design of additive quantum codes via the code-word-stabilized framework, *Phys. Rev. A* **84**, 062319 (2011).
- [16] B. M. Terhal, F. Hassler, and D. P. DiVincenzo, From Majorana fermions to topological order, *Phys. Rev. Lett.* **108**, 260504 (2012).
- [17] J. Bonilla Ataides, D. Tuckett, S. Bartlett, S. Flammia, and B. Brown, The XZZX surface code, *Nat. Commun.* **12**, 1 (2021).
- [18] D. J. C. MacKay, G. Mitchison, and P. L. McFadden, Sparse-graph codes for quantum error correction, *IEEE Trans. Inf. Theory* **50**, 2315 (2004).
- [19] J.-P. Tillich and G. Zémor, Quantum LDPC codes with positive rate and minimum distance proportional to the square root of the block-length, *IEEE Trans. Inf. Theory* **60**, 1193 (2014).
- [20] A. A. Kovalev and L. P. Pryadko, Quantum Kronecker sum-product low-density parity-check codes with finite rate, *Phys. Rev. A* **88**, 012311 (2013).
- [21] P. Pantelev and G. Kalachev, Quantum LDPC codes with almost linear minimum distance, *IEEE Trans. Inf. Theory* **68**, 213 (2022).
- [22] D. Gottesman, Fault-tolerant quantum computation with constant overhead, *Quantum Inf. Comput.* **14**, 1338 (2014).
- [23] N. P. Breuckmann and J. N. Eberhardt, Quantum low-density parity-check codes, *PRX Quantum* **2**, 040101 (2021).
- [24] C.-Y. Lai and K.-Y. Kuo, Harnessing coding theory for reliable network quantum communication, *IEEE Wireless Commun.* **31**, 82 (2024).
- [25] A. Zaidi, F. Athley, J. Medbo, U. Gustavsson, G. Durisi, and X. Chen, *5G Physical Layer: principles, models and technology components* (Academic Press, 2018).
- [26] K. Arora, J. Singh, and Y. S. Randhawa, A survey on channel coding techniques for 5G wireless networks, *Telecommun. Syst.* **73**, 637 (2020).
- [27] M. Sipser and D. A. Spielman, Expander codes, *IEEE Trans. Inf. Theory* **42**, 1710 (1996).
- [28] M. G. Luby, M. Mitzenmacher, M. A. Shokrollahi, and D. A. Spielman, Efficient erasure correcting codes, *IEEE Trans. Inf. Theory* **47**, 569 (2001).
- [29] C. Di, D. Proietti, I. E. Telatar, T. J. Richardson, and R. L. Urbanke, Finite-length analysis of low-density parity-check codes on the binary erasure channel, *IEEE Trans. Inf. Theory* **48**, 1570 (2002).
- [30] T. J. Richardson and R. L. Urbanke, Efficient encoding of low-density parity-check codes, *IEEE Trans. Inf. Theory* **47**, 638 (2001).
- [31] D. J. C. MacKay and M. S. Postol, Weaknesses of Margulis and Ramanujan-Margulis low-density parity-check codes, *Electron. Notes Theor. Comput. Sci.* **74**, 97 (2003).
- [32] R. M. Tanner, D. Sridhara, A. Sridharan, T. E. Fuja, and D. J. Costello, LDPC block and convolutional codes based on circulant matrices, *IEEE Trans. Inf. Theory* **50**, 2966 (2004).
- [33] A. Shokrollahi, Raptor codes, *IEEE Trans. Inf. Theory* **52**, 2551 (2006), see also <http://dx.doi.org/10.1561/01000000060>.
- [34] N. Connolly, V. Londe, A. Leverrier, and N. Delfosse, Fast erasure decoder for hypergraph product codes, *Quantum* **8**, 1450 (2024).
- [35] T. Richardson, Error floors of LDPC codes, in *Proc. Annu. Allerton Conf. Commun., Control, Comput.*, Vol. 41 (2003) pp. 1426–1435.
- [36] A. Orliutsky, R. Urbanke, K. Viswanathan, and J. Zhang, Stopping sets and the girth of Tanner graphs, in *Proc. IEEE Int. Symp. Inf. Theory (ISIT)* (2002) p. 2.
- [37] N. Delfosse and G. Zémor, Linear-time maximum likelihood decoding of surface codes over the quantum erasure channel, *Phys. Rev. Res.* **2**, 033042 (2020).
- [38] A. B. Alosious and P. K. Sarvepalli, Erasure decoding of two-dimensional color codes, *Phys. Rev. A* **100**, 042312 (2019).
- [39] H. M. Solanki and P. K. Sarvepalli, Decoding topological subsystem color codes over the erasure channel using gauge fixing, *IEEE Trans. Commun.* **71**, 4181 (2023).
- [40] S. Lee, M. Mhalla, and V. Savin, Trimming decoding of color codes over the quantum erasure channel, in *Proc. IEEE Int. Symp. Inf. Theory (ISIT)* (2020) pp. 1886–1890.
- [41] M. Kang, W. C. Campbell, and K. R. Brown, Quantum error correction with metastable states of trapped ions using erasure conversion, *PRX Quantum* **4**, 020358 (2023).
- [42] K. Sahay, J. Jin, J. Claes, J. D. Thompson, and S. Puri, High-threshold codes for neutral-atom qubits with biased erasure errors, *Phys. Rev. X* **13**, 041013 (2023).
- [43] J. Edmonds, Paths, trees, and flowers, *Can. J. Math.* **17**, 449 (1965).
- [44] D. Poulin and Y. Chung, On the iterative decoding of sparse quantum codes, *Quantum Inf. Comput.* **8**, 987 (2008).
- [45] K.-Y. Kuo and C.-Y. Lai, Exploiting degeneracy in belief propagation decoding of quantum codes, *npj Quantum Inf.* **8**, art. no. 111 (2022), (See also the arXiv version: <https://arxiv.org/abs/2104.13659>).
- [46] R. G. Gallager, *Low-Density Parity-Check Codes*, no. 21 in Research Monograph Series (MIT Press, 1963).
- [47] D. J. C. MacKay, Good error-correcting codes based on very sparse matrices, *IEEE Trans. Inf. Theory* **45**, 399 (1999).
- [48] K.-Y. Kuo and C.-Y. Lai, Refined belief propagation decoding of sparse-graph quantum codes, *IEEE J. Sel. Areas Inf. Theory* **1**, 487 (2020).
- [49] Y. Ouyang, Permutation-invariant quantum codes, *Phys. Rev. A* **90**, 062317 (2014).
- [50] Y. Ouyang, Permutation-invariant quantum coding for quantum deletion channels, in *Proc. IEEE Int. Symp. Inf. Theory (ISIT)* (2021) pp. 1499–1503.
- [51] A. R. Calderbank, E. M. Rains, P. W. Shor, and N. J. A. Sloane, Quantum error correction via codes over GF(4), *IEEE Trans. Inf. Theory*

- 44, 1369 (1998).
- [52] D. Gottesman, *Stabilizer codes and quantum error correction*, Ph.D. thesis, California Institute of Technology (1997).
- [53] M. A. Nielsen and I. L. Chuang, *Quantum Computation and Quantum Information* (Cambridge University Press, 2000).
- [54] A. R. Calderbank and P. W. Shor, Good quantum error-correcting codes exist, *Phys. Rev. A* **54**, 1098 (1996).
- [55] A. M. Steane, Error correcting codes in quantum theory, *Phys. Rev. Lett.* **77**, 793 (1996).
- [56] M.-H. Hsieh and F. L. Gall, NP-hardness of decoding quantum error-correction codes, *Phys. Rev. A* **83**, 052331 (2011).
- [57] P. Iyer and D. Poulin, Hardness of decoding quantum stabilizer codes, *IEEE Trans. Inf. Theory* **61**, 5209 (2015).
- [58] K.-Y. Kuo and C.-C. Lu, On the hardnesses of several quantum decoding problems, *Quantum Inf. Process.* **19**, 1 (2020).
- [59] N. Delfosse and G. Zémor, Upper bounds on the rate of low density stabilizer codes for the quantum erasure channel, *Quantum Info. Comput.* **13**, 793–826 (2013).
- [60] M. Grassl, T. Beth, and T. Pellizzari, Codes for the quantum erasure channel, *Phys. Rev. A* **56**, 33 (1997).
- [61] F. J. MacWilliams and N. J. A. Sloane, *The Theory of Error-Correcting Codes* (North-Holland Publishing Company, 1977).
- [62] W. Hoeffding, Probability inequalities for sums of bounded random variables, *J. Am. Stat. Assoc.*, 13 (1963).
- [63] R. Cleve and D. Gottesman, Efficient computations of encodings for quantum error correction, *Phys. Rev. A* **56**, 76 (1997).
- [64] J. Pearl, *Probabilistic reasoning in intelligent systems: networks of plausible inference* (Morgan Kaufmann, 1988).
- [65] R. Tanner, A recursive approach to low complexity codes, *IEEE Trans. Inf. Theory* **27**, 533 (1981).
- [66] F. R. Kschischang, B. J. Frey, and H.-A. Loeliger, Factor graphs and the sum-product algorithm, *IEEE Trans. Inf. Theory* **47**, 498 (2001).
- [67] C.-Y. Lai and K.-Y. Kuo, Log-domain decoding of quantum LDPC codes over binary finite fields, *IEEE Trans. Quantum Eng.* **2**, art. no. 2103615 (2021).
- [68] J. J. Hopfield, Neurons with graded response have collective computational properties like those of two-state neurons, *Proc. Nat. Acad. Sci. (PNAS)* **81**, 3088 (1984).
- [69] J. J. Hopfield and D. W. Tank, “neural” computation of decisions in optimization problems, *Biol. Cybern.* **52**, 141 (1985).
- [70] J. J. Hopfield and D. W. Tank, Computing with neural circuits: A model, *Science* **233**, 625 (1986).
- [71] M. Fossorier and S. Lin, Soft-decision decoding of linear block codes based on ordered statistics, *IEEE Trans. Inf. Theory* **41**, 1379 (1995).
- [72] P. Panteleev and G. Kalachev, Degenerate quantum LDPC codes with good finite length performance, *Quantum* **5**, 585 (2021).
- [73] J. Roffe, D. R. White, S. Burton, and E. T. Campbell, Decoding across the quantum low-density parity-check code landscape, *Phys. Rev. Res.* **2**, 043423 (2020).
- [74] J. Chen and M. P. C. Fossorier, Density evolution for two improved BP-based decoding algorithms of LDPC codes, *IEEE Commun. Lett.* **6**, 208 (2002).
- [75] J. Chen, A. Dholakia, E. Eleftheriou, M. P. C. Fossorier, and X.-Y. Hu, Reduced-complexity decoding of LDPC codes, *IEEE Trans. Commun.* **53**, 1288 (2005).
- [76] K. Kasai, M. Hagiwara, H. Imai, and K. Sakaniwa, Quantum error correction beyond the bounded distance decoding limit, *IEEE Trans. Inf. Theory* **58**, 1223 (2011).
- [77] M. P. C. Fossorier, Quasi-cyclic low-density parity-check codes from circulant permutation matrices, *IEEE Trans. Inf. Theory* **50**, 1788 (2004).
- [78] N. Raveendran, N. Rengaswamy, F. Rozpędek, A. Raina, L. Jiang, and B. Vasić, Finite rate QLDPC-GKP coding scheme that surpasses the CSS Hamming bound, *Quantum* **6**, 767 (2022).
- [79] T. J. Richardson, M. A. Shokrollahi, and R. L. Urbanke, Design of capacity-approaching irregular low-density parity-check codes, *IEEE Trans. Inf. Theory* **47**, 619 (2001).
- [80] G. A. Malema, *Low-density parity-check codes: construction and implementation*, Ph.D. thesis, University of Adelaide, SA, Australia (2007).
- [81] K.-Y. Kuo and C.-Y. Lai, Comparison of 2D topological codes and their decoding performances, in *Proc. IEEE Int. Symp. Inf. Theory (ISIT)* (2022) pp. 186–191.
- [82] T. M. Stace, S. D. Barrett, and A. C. Doherty, Thresholds for topological codes in the presence of loss, *Physical review letters* **102**, 200501 (2009).
- [83] M. Ohzeki, Error threshold estimates for surface code with loss of qubits, *Phys. Rev. A* **85**, 060301 (2012).
- [84] D. Bluvstein, H. Levine, G. Semeghini, T. T. Wang, S. Ebadi, M. Kalinowski, A. Keesling, N. Maskara, H. Pichler, M. Greiner, *et al.*, A quantum processor based on coherent transport of entangled atom arrays, *Nature* **604**, 451 (2022).
- [85] M. B. Ruskai, Pauli Exchange Errors in Quantum Computation, *Physical Review Letters* **85**, 194 (2000).
- [86] H. Pollatsek and M. B. Ruskai, Permutationally invariant codes for quantum error correction, *Linear Algebra and its Applications* **392**, 255 (2004).
- [87] Y. Ouyang and J. Fitzsimons, Permutation-invariant codes encoding more than one qubit, *Physical Review A* **93**, 042340 (2016).
- [88] Y. Ouyang, Permutation-invariant qudit codes from polynomials, *Linear Algebra and its Applications* **532**, 43 (2017).
- [89] T. Shibayama and M. Hagiwara, Permutation-invariant quantum codes for deletion errors, in *2021 IEEE International Symposium on Information Theory (ISIT)* (2021) pp. 1493–1498.
- [90] A. Nakayama and M. Hagiwara, The first quantum error-correcting code for single deletion errors, *IEICE Communications Express* **9**, 100 (2020).
- [91] M. Hagiwara and A. Nakayama, A four-qubits code that is a quantum deletion error-correcting code with the optimal length, in *IEEE International Symposium on Information Theory, ISIT 2020, Los Angeles, CA, USA, June 21-26, 2020* (IEEE, 2020) pp. 1870–1874.
- [92] A. Aydin, M. A. Alekseyev, and A. Barg, A family of permutationally invariant quantum codes, *Quantum* **8**, 1321 (2024).